Available online at www.sciencedirect.com
ScienceDirect
Journal of Computational Physics 227 (2008) 2212–2237
JOURNAL OF COMPUTATIONAL PHYSICS
www.elsevier.com/locate/jcp

A 3-D multiband closure for radiation and neutron transfer moment models

J.-F. Ripoll [a,*], A.A. Wray [b]

[a] Center for Turbulence Research, Stanford University, Stanford, CA 94305, USA
[b] NASA Ames Research Center, Moffett Field, CA 94035, USA

Received 23 January 2007; received in revised form 15 August 2007; accepted 27 August 2007
Available online 22 September 2007

Abstract

We derive a 3D multi-band moment model and its associated closure for radiation and neutron transfer. The new closure is analytical and nonlinear but very simple. Its derivation is based on the maximum entropy closure and assumes a Wien shape for the intensity when used in the Eddington tensor. In the multi-band approach, the opacity is re-arranged (binned) according to the opacity value. The multi-band model propagates identically all photons/neutrons having the same opacity. This has been found to be a good approximation on average since the transport is mostly determined by the opacities and less by the frequencies. This same concept is used to derive the closure. We prove on two complex test atmospheres (the solar atmosphere and an artificial atmosphere) that the closure we have derived has good accuracy. All approximations made in deriving the model have been carefully numerically checked and quantified.
Published by Elsevier Inc.

Keywords: Radiative transfer; Neutron transfer; Moment models; Maximum entropy closure; Multi-band models; ODF; Multi-bin models

1. Introduction

When computing radiation or neutron transfer one is tempted to use macroscopic moment models since theoretically they carry a much lower computational cost than does direct solution of the radiative transfer equation (RTE). In radiative transfer, they have been used in many applications related to combustion, cloud physics, astrophysics, heat transfer, and in problems involving the coupling of radiation with other large sets of equations [1–5]. Similarly, for neutron transfer (for which the transfer law is very similar to the RTE) these methods have also been frequently used because of their lower cost [6–8]. In all these applications, the steady diffusion formulation was most often used, and the closure chosen was P_1, i.e. $\mathbf{P}_R = \mathbf{1/3}E_R$ where E_R and $\mathbf{P}_R$ denote the radiative energy and pressure tensor, respectively.

* Corresponding author. Present address: Space and Remote Sensing Sciences (ISR-2), Los Alamos National Laboratory, MS D436, P.O. Box 1663, NM 87545, USA. Tel.: +1 505 667 5992; fax: +1 505 664 0362.
E-mail addresses: ripoll@lanl.gov (J.-F. Ripoll), wray@nas.nasa.gov (A.A. Wray).

0021-9991/$ - see front matter Published by Elsevier Inc.
doi:10.1016/j.jcp.2007.08.028

In the derivation of usual moment models and in their closures, the frequency integration is either analytically performed over the whole frequency spectrum (gray case) [9,10,17] or not performed at all (monochromatic case) [27,28]. The use of these models is then theoretically limited to gray/monochromatic cases. The goal of this paper is to derive a valid moment model and its closure for the case of general non-gray media.

As the reader may know, the closure model, i.e. Eddington tensor[1] $\mathbf{D}_R$ contained in the model $\mathbf{P}_R = \mathbf{D}_R E_R$, is the crucial modeling step required in the moment formulation. It must guarantee the correct speed (bounded by the speed of light) and direction of propagation for the photons/neutrons, and it strongly affects the accuracy of the modeling. This term can be seen as a *flux limiter* [11–13,9], because one of its roles is to limit the propagation of the flux. Pioneering work in the 1970s on flux limiters is well referenced in [14] (see also [3, p. 479] and [15]). Flux limiters were introduced because simple closures such as P_1 violate the flux limit $F_R < cE_R$ in transparent media. The accuracy is then low unless the transport is nearly isotropic [16,3,17–19]. This has been well known for many years; for instance in [16, p. 148], the author noted ...*The interface between a fluid and a vacuum requires special examination. Since the vacuum does not supply any photons, the radiation field at the interface is strongly anisotropic (all photons travel only in the direction toward the vaccum), and, strictly speaking the diffusion application is inapplicable.*[2] As a result, most recent numerical algorithms always try to incorporate flux limiters [20–24,14,25,26] as they are required for the accuracy of the solution.

The main focus over the past twenty five years has been to improve the closure models of moment methods for simple gray/monochromatic media, and much has been achieved [27,13,9,12,10,29–31,28,32,17]. Greater generality is now possible in the non-gray case. In particular, techniques developed for deriving closure models on full-spectrum problems, such as the maximum entropy concept [27], can be applied to the derivation of by-band or by-group closure models. This development is also encouraged by recent accurate results found in the gray case [17,34] for various multi-dimensional configurations.

For non-gray problems, the spectral dependence of the opacity is handled either through multi-group or multi-band divisions. The present work will contribute to developing moment methods in the multi-band framework. For the multi-group case, the reader should refer to [35,36,33]. However, the derivation of non-gray moment models is not straightforward; the Eddington tensor is much more complex since the integration over frequency cannot be done analytically except in special cases. Recently in [35] (see also references therein) this subject has been treated by a *new consistent multi-group moment model*. In that work, the frequency domain is divided into n groups, and a moment system is derived for each group. The radiative pressure is closed by a model using the maximum entropy closure [27,31,28]. A complex mathematical formulation is then used by the author to approximate the required integrals over each frequency group and angle. (The closure is, surprisingly, not explicitly written in [35]; we found it in [36, pp. 52–59]). Unfortunately, it leads to a non-analytical model (see also [33] where a similar closure is derived based on half-moments [32,17]). The mathematical reason is related to the fact that the integral $\int_{\nu_0}^{\nu_1} \mathcal{B}(T,\nu)\mathrm{d}\nu$, where $\mathcal{B}(T,\nu)$ is the Planck function, does not admit a known closed form for ν_0 and ν_1 finite (see [5, p. 11]). The great complexity of this model and the lack of evidence of its accuracy have encouraged us to derive a simpler multi-band moment model which we now describe.

Our approach is dictated by the fact that we wish to avoid handling integrals $\int_{\nu_0}^{\nu_1}$ in order to be able to derive a closed-form closure. As a result, we choose to divide the opacity space $\{\sigma(\nu)\}$ into n bins (or bands) $\{\sigma \in [0, +\infty]\}$. An opacity bin (or band) corresponds in general to disjoint sets of frequencies. For this reason, and contrary to our title, the method presented here will be referred to from now on as a *by-bin* or *multi-bin* method, rather than as a by-band or multi-band method.

Binning is an old idea which consists in creating *photon bins* in which the frequencies ν in the whole spectrum (or in a contiguous subset) are regrouped according to the value of the opacities at those frequencies. The general technique is referred to as the *opacity distribution function (ODF)* in [3, p. 365–366] (and references therein). The original idea is attributed to Chandrasekhar in [37] by Kurucz ([38]), who uses the method in his ATLAS codes [39] for providing absorption coefficients for a large variety of stars [40]. The ODF was used in the early seventies [38,40,39,42,41] and is commonly used today in [48,43,44,46,47,45]. In [38,41,3,43,45], the

[1] This term is also referred to as the *pressure closure*, *Eddington tensor*, *closure model* or *term*, or as *flux limiter* since it acts like one.

[2] The word *diffusion* denotes in the author's context the P_1 diffusion formulation.

bins are called *pickets*, while the word *bin* has been used as a verb in [3, p. 365]. Binning by opacity instead of grouping by frequency has long been used for solar simulations (see for instance [48,50,51,49,52,53] and references therein). We have also recently used this approach to re-entry problems [54,55]. In those works, in [46,47], and in this paper, the binning is done over the whole spectrum. In the multi-band method ([56] and references therein), or in the ODF method, the same rearrangement is usually done inside each of n_g groups. For simplicity, in the present work we use the multi-band, or equivalently the ODF method, with $n_g = 1$. However, we will see in Section 5.5 that this is not mandatory; our model is fully general and can be used for $n_g \neq 1$, provided there are enough frequencies in a group to guarantee a coherent binning. A by-bin re-arrangement of the opacity is also performed on the whole spectrum in the FSK method [57,5], where a PDF is introduced and smooths the opacity. Similarly, smooth, weighted re-arrangements of the opacity are also proposed in [58,59] and in [60]. The goal of the current paper is not to detail or discuss those techniques but to provide a multi-band/bin/picket moment system usable in combination with any rearrangement of the frequency according to the opacity value.

The subdivision of the frequency space into opacity bins modifies the definitions of the moments: integrals over a range of frequencies, e.g. $\int_{\nu_i}^{\nu_{i+1}}$, become summations over sets of scattered frequencies: $\sum_{\nu\in\nu^i}$. The by-bin method conceptually offers three main advantages. First, it is easy to retain all frequencies in the model, which allows a full description of the medium; for instance one can use five bins following the opacity scales of the problem (e.g., very opaque, opaque, semi transparent, mostly transparent, and transparent [3, p. 365]). Second, for very low or high opacities the closure model is essentially exact; that is, there exist $\sigma_{\min}$ and $\sigma_{\max}$ for which the Eddington factor (cf. Eq. (22) for the exact definition) $\chi^\sigma \simeq 1/3$ for $\sigma > \sigma_{\max}$, and $\chi^\sigma \simeq 1$ for $\sigma < \sigma_{\min}$. This is because the opacity binning will automatically sort the anisotropies f such that: $f^\sigma \simeq 0$ for $\sigma > \sigma_{\max}$ and $f^\sigma \simeq 1$ for $\sigma < \sigma_{\min}$ (cf. text below Eq. (22) for the exact definition of the anisotropies f). Third, and most importantly, such a division will prevent the occurrence of a huge range of values of the anisotropy factor inside a given bin, and consequently prevent a huge range of values of the Eddington tensor. The two last remarks are related to the fact that *transport depends on the value of the opacity not the value of the frequency*, as well summarized in [45]. This will lead to a more accurate closure, as we now sketch.

When a standard frequency grouping is done, the variation of the local opacity, σ^ν, can be very large inside a group. As a result, the local anisotropy factor, f^ν, will vary over its full range, from 0 to 1, as will the Eddington tensor closure χ^ν, from 1/3 to 1. The chosen mean value χ^g, taken to represent the group, must account for a set of χ^ν covering this range. The resulting error due to the modeling is then likely to be high because of the large differences between the mean and the specific ν-values.[3] On the other hand, when an opacity binning is done, only small variations of the anisotropy factors f^ν inside a bin are expected. In consequence, small variations of the Eddington factors in the bin should follow, avoiding strong deviations between the mean value in the bin, χ^b, and the sample values, χ^ν, leading to better accuracy. The actual situation is somewhat more complex than this sketch describes, as we will see in our numerical examples, but the main concepts remain.

The downsides to this method are dealing with disjoint sets of ν's and the requirement to make two kinds of approximations. First, to achieve our goal of finding a simple and closed-form closure model, an approximation to the ideal maximum-entropy pseudo-intensity will be used in the radiative case: it is assumed that the Planck-form pseudo-intensity can be approximated by a Wien form I_{w}. For neutron transport, this is not an approximation since this form follows directly from the use of the maximum entropy closure [27,28,61]. However, for radiative transfer it should theoretically hold only when $h\nu/(kT) \gg 1$. We will prove numerically that, when used to close the Eddington tensor, i.e. $\int_\Omega I_{\mathrm{w}}\Omega^2\,\mathrm{d}\Omega / \int_\Omega I_{\mathrm{w}}\,\mathrm{d}\Omega$, this approximation is valid. If one wants to avoid this approximation, the integral of the full pseudo-intensity may be done numerically (at high cost), as in [36], but we achieve good numerical results without the very complex formulation and cost of that work.

The second required approximation is that the mean radiative anisotropy and Eddington factor in a bin, f^{b} and χ^b, are assumed to be representative of the average of all f^ν and χ^ν in the bin. We believe this approximation can be done in a by-bin framework, while it cannot be done in a by-group division (as explained two paragraphs above). These approximations are needed to derive the closure. They will be specifically tested numerically and shown to be reasonable. In the limit where there are as many bins as frequencies, it will

[3] In most Eddington factor models the loss of accuracy occurs in transition zones since both limits 1/3 and 1 are exact.

be shown that the closure derived here is the one derived first by Minerbo [27] for radiation and later on by Brunner and Holloway [28] for neutron transport. Both derivations were done in the monochromatic case, and the only approximation they made is the Wien form of the pseudo-intensity, which comes from the maximum entropy closure. But when the medium is strongly dependent on the frequency, a large number of frequencies is needed to resolve the dependence, and solving one moment model per discrete frequency has too a high computational cost.

Two numerical problems of radiative transfer (the neutron case contains fewer approximations) will be considered. First, a 1D *realistic* spherically symmetric model of the atmosphere of the sun will be considered. The opacity and temperature profiles of this atmosphere have been provided by Stein and Nordlund [48,50,51,49,52]. It is composed of 2748 frequencies. The opacity profile is strongly dependent on the frequency, leading to a challenging modeling problem. It will be shown that the closure model is accurate (less than 10% error in overall average when using all 2748 frequency bins, thus proving that the Wien form of the pseudo-intensity, which is the only approximation made in this case, constitutes a valid approximation for radiative transfer at these temperatures and frequencies.

For smaller numbers of bins reasonable accuracy is also obtained, even in the limit of as few as 5–10 bins (if they are correctly chosen). This result gives confidence that, along with the by-bin closure, the approximations made *inside* a bin are reasonable as well. The model is also found usable for computing the radiation in the solar chromosphere.

The second test case is the same solar atmosphere modified in scale by decreasing the radius of the atmosphere. This produces much more anisotropic radiation as a challenge to the model. The closure model is also found acceptably accurate.

In addition it will be demonstrated that the new closure constitutes a great improvement compared to the P_1 model, the accuracy of which is found to be very poor. We will also show that no major numerical difficulty or cost is introduced by the non-analytic form of the closure model; the Newton's method solution required by the closure takes only a few iterations (<10).

The article is organized as follows. In Sections 2 and 3, the various definitions and the binning are introduced. The by-bin moment model is derived in Section 4, and its closure is described in Section 5. In Section 6, the numerical results are presented.

2. The radiative transfer equation

The radiative transfer equation in a non-scattering, emitting, and absorbing non-gray medium is given by

$$\frac{1}{c}\partial_t I + \mathbf{\Omega}\cdot\nabla I = \sigma(\nu)\mathcal{B}(\nu,T) - \sigma(\nu)I, \tag{1}$$

where the intensity $I = I(t, \mathbf{r}, \mathbf{\Omega}, \nu)$ is a function of the time t, the position $\mathbf{r}$, the direction of propagation $\mathbf{\Omega}$, and the frequency ν. Here c is the velocity of light and $\sigma(\nu)$, the spectral absorption coefficient or opacity, is assumed strongly dependent on ν. The Planck radiative intensity $\mathcal{B}$ describes the isotropic emission of the medium at frequency ν and temperature T by

$$\mathcal{B}(\nu,T) = \frac{2h\nu^3}{c^2}\left[\exp\left(\frac{h\nu}{kT}\right) - 1\right]^{-1}, \tag{2}$$

where h is the Planck constant and k the Boltzmann constant.

3. Definitions

Given a medium of opacity $\sigma(\nu) \in [0, \infty]$ for $\nu \in [0, \infty]$, we divide the range of values of σ into n bins by choosing $n+1$ distinct increasing numbers $b_{i+\frac{1}{2}}$ for $i = 0, \ldots, n$. These b are the boundary values of the bins in σ-space with $b_{\frac{1}{2}} = 0$ and $b_{n+\frac{1}{2}} = \infty$. We will refer to the range of $\sigma \in \left[b_{i-\frac{1}{2}}, b_{i+\frac{1}{2}}\right)$ as the ith bin. Spatially constant $b_{i+\frac{1}{2}}$ will be used in the present work; the case of spatially varying bins will be addressed in another article, but it should be noted that spatial dependence does not affect the main focus of this paper, which is the derivation of the closure. For instance, the non-constant case introduces extra source-terms to transfer rays from

one bin to another as they move through space [56]. The numerical tests on the closure will be performed using a spatially dependent opacity but spatially fixed b by using a spatial average of $\sigma(\nu, \mathbf{x})$ to define the bins.

For purposes of simulation, frequency space is discretized into a set of values ν_j, each representing a small range of frequencies $\nu_j - \Delta\nu/2 \leqslant \nu < \nu_j + \Delta\nu/2$. The set of frequencies in the ith bin is then represented by some subset ν_{i_k}:

$$\{\nu_{i_k}, k = 1, \ldots, k_{\max}\} = \left\{\nu_j | \sigma(\nu_j) \in \left[b_{i-\frac{1}{2}}, b_{i+\frac{1}{2}}\right)\right\}. \tag{3}$$

In general, the number of frequency samples per bin, $k_{\max}$, will vary from bin to bin. For all frequencies ν in the ith bin, $\sigma(\nu)$ will be approximated as $\sigma(\nu) \approx \bar{\sigma}_i$, where the mean opacity in the ith bin, $\bar{\sigma}_i$, is taken to be either the simple arithmetic mean or some more complex mean [62–64] over the bin.

We now give some notational abbreviations to simplify the expressions to follow. We will denote the integration of a function f over 4π steradians of direction as $\langle f\rangle_\Omega$ and that over the frequency interval $\nu_i - \Delta\nu/2$ to $\nu_i + \Delta\nu/2$ as $\langle f\rangle_{\nu_i}$; a summation over the discrete frequencies ν_{i_k} in the ith bin will be written as $\sum_{i_k}$; finally, a quantity computed inside the ith bin will be denoted by a superscript i.

The by-bin moments for the ith bin are defined by

$$E_R^i(t, \mathbf{r}) = \frac{1}{c}\sum_{i_k}\left\langle \int_{\nu_{i_k}-\Delta\nu/2}^{\nu_{i_k}+\Delta\nu/2} I(t, \mathbf{r}, \boldsymbol{\Omega}, \nu)\mathrm{d}\nu \right\rangle_\Omega = \frac{1}{c}\sum_{i_k}\langle I\rangle_{\Omega,\nu_{i_k}} \tag{4}$$

$$\mathbf{F}_R^i(t, \mathbf{r}) = \sum_{i_k}\left\langle \int_{\nu_{i_k}-\Delta\nu/2}^{\nu_{i_k}+\Delta\nu/2} \boldsymbol{\Omega} I(t, \mathbf{r}, \boldsymbol{\Omega}, \nu_{i_k})\mathrm{d}\nu \right\rangle_\Omega = \sum_{i_k}\langle \boldsymbol{\Omega} I\rangle_{\Omega,\nu_{i_k}} \tag{5}$$

$$\mathbf{P}_R^i(t, \mathbf{r}) = \frac{1}{c}\sum_{i_k}\left\langle \int_{\nu_{i_k}-\Delta\nu/2}^{\nu_{i_k}+\Delta\nu/2} \boldsymbol{\Omega}\otimes\boldsymbol{\Omega} I(t, \mathbf{r}, \boldsymbol{\Omega}, \nu_{i_k})\mathrm{d}\nu \right\rangle_\Omega \tag{6}$$

$$= \frac{1}{c}\sum_{i_k}\langle \boldsymbol{\Omega}\otimes\boldsymbol{\Omega} I\rangle_{\Omega,\nu_{i_k}} \tag{7}$$

In the limit $\Delta\nu \to 0$ the first of these becomes

$$E_R^i(t, \mathbf{r}) = \frac{1}{c}\sum_{i_k}\lim_{\Delta\nu\to 0}\int_{\nu_{i_k}-\Delta\nu/2}^{\nu_{i_k}+\Delta\nu/2}\langle I(t, \mathbf{r}, \boldsymbol{\Omega}, \nu)\rangle_\Omega \mathrm{d}\nu \tag{8}$$

$$= \frac{1}{c}\sum_{i_k}\Delta\nu\int_0^\infty \langle I(t, \mathbf{r}, \boldsymbol{\Omega}, \nu)\rangle_\Omega \delta(\nu - \nu_{i_k})\mathrm{d}\nu \tag{9}$$

which is the formulation usually adopted [56].

The full moments are derived from the bin-moments by summing over all bins: $E_R = \sum_{i=1}^n E_R^i$, $\mathbf{F}_R = \sum_{i=1}^n \mathbf{F}_R^i$ and $\mathbf{P}_R = \sum_{i=1}^n \mathbf{P}_R^i$.

4. Derivation of the by-bin moment model

Integrating the radiative transfer Eq. (1) over direction, over frequency interval $\Delta\nu$, and summing over the disjoint set ν_{i_k} of ν's which define the bin i, one obtains

$$\partial_t \frac{1}{c}\sum_{i_k}\langle I(t, \mathbf{r}, \boldsymbol{\Omega}, \nu_{i_k})\rangle_{\Omega,\nu_{i_k}} + \nabla\cdot\sum_{i_k}\langle \boldsymbol{\Omega} I(t, \mathbf{r}, \boldsymbol{\Omega}, \nu_{i_k})\rangle_{\Omega,\nu_{i_k}} \tag{10}$$

$$= \sum_{i_k}\langle \sigma(\nu_{i_k})\mathcal{B}(T, \nu_{i_k})\rangle_{\Omega,\nu_{i_k}} - \sum_{i_k}\langle \sigma(\nu_{i_k}) I(t, \mathbf{r}, \boldsymbol{\Omega}, \nu_{i_k})\rangle_{\Omega,\nu_{i_k}} \tag{11}$$

The sum and partial differential operators commute since the binning does not depend on position or time. As mentioned above, the opacity $\sigma(\nu_{i_k})$ in a bin is either approximated by an average value or by a mean coefficient, both denoted here $\bar{\sigma}_i$; it is independent of ν. Thus Eq. (11) becomes

$$\partial_t E_R^i + \nabla\cdot\mathbf{F}_R^i = c4\pi\bar{\sigma}_i S^i - c\bar{\sigma}_i E_R^i, \tag{12}$$

where $S^i = \sum_{i_k}\mathcal{B}(T, \nu_{i_k})$.

Multiplying the radiative transfer Eq. (1) by $\mathbf{\Omega}$ and integrating as before leads to

$$\partial_t \frac{1}{c}\sum_{i_k}\langle \mathbf{\Omega} I(t,\mathbf{r},\mathbf{\Omega},\nu_{i_k})\rangle_{\Omega,\nu_{i_k}} + \nabla\cdot\sum_{i_k}\langle \mathbf{\Omega}\otimes\mathbf{\Omega} I(t,\mathbf{r},\mathbf{\Omega},\nu_{i_k})\rangle_{\Omega,\nu_{i_k}} \tag{13}$$

$$= -\sum_{i_k}\langle \sigma(\nu_{i_k})\mathbf{\Omega} I(t,\mathbf{r},\mathbf{\Omega},\nu_{i_k})\rangle_{\Omega,\nu_{i_k}} \tag{14}$$

which, with the same arguments, leads to

$$\frac{1}{c}\partial_t \mathbf{F}_R^i + c\nabla\cdot\mathbf{P}_R^i = -\bar{\sigma}^i\mathbf{F}_R^i. \tag{15}$$

The multi-band (or by-bin) moment model consists of the two equations (12) and (15) describing the evolution of the by-bin energy and flux. To close the system, a model for the radiative pressure as a function of these two moments is presented in the following section.

5. Derivation of the by-bin model closure

It is assumed that, for the purpose of modeling the radiative pressure, the intensity in the ith bin, $I^i = I(t,\mathbf{r},\mathbf{\Omega},\nu)$, can be approximated by a prescribed function $I_*^i(t,\mathbf{r},\mathbf{\Omega},\nu)$ for all ν in the bin. The form of this function is taken to be the maximum entropy closure [27,31] for radiative transfer where the entropy function used for photons is the Bose–Einstein one [61]. The maximum entropy result for the intensity is

$$I_*^i(t,\mathbf{r},\mathbf{\Omega},\nu) = \frac{2h\nu^3}{c^2}\left[\exp\left(\frac{h\nu}{k}A^i(1-\mathbf{B}^i\cdot\mathbf{\Omega})\right)-1\right]^{-1} \tag{16}$$

The scalar and vector coefficients, A^i and $\mathbf{B}^i$, are computed from the two constraints $E_R^i = 1/c\sum_{i_k}\langle I_*^i\rangle_{\mathbf{\Omega},\nu_{i_k}}$ and $\mathbf{F}_R^i = \sum_{i_k}\langle \mathbf{\Omega} I_*^i\rangle_{\mathbf{\Omega},\nu_{i_k}}$ (as done for instance in [27,31,28,17] for the gray/monochromatic case).

Some remarks should be made here which distinguish this work from the gray/monochromatic case. For a given bin i, the intensity I^i and its approximation I_*^i are functions of ν for that bin. However, the coefficients A^i and $\mathbf{B}^i$ do not depend on frequency and are constant throughout the bin. Thus, in order that the intensity for each ν in the bin be accurately represented, it is important to have accurate values of these moments; this is easier in a by-bin framework than in a by-group one.

It could be assumed that $\mathbf{P}_R^i \simeq \frac{1}{c}\sum_{i_k}\langle \mathbf{\Omega}\otimes\mathbf{\Omega} I_*^i\rangle_{\Omega,\nu_{i_k}}$. Unfortunately, the intensity (16) does not lead to a closed form expression when used in the pressure expression. There are two alternatives at this point. One could choose to carry an approximation of the integral as done in [36]; this leads in our opinion to too complex a form of the model. Alternatively, one can try to simplify the function I_*^i which must be integrated. This approach, which we follow here, has the advantage of leading to a simpler final pressure model, but it does require approximation of the integrand. We hence approximate the Planck intensity function by the Wien form:

$$I_*^i \simeq I_w^i(t,\mathbf{r},\mathbf{\Omega},\nu) = \frac{2h\nu^3}{c^2}\left[\exp\left(\frac{h\nu}{k}A^i(1-\mathbf{B}^i\cdot\mathbf{\Omega})\right)\right]^{-1} \tag{17}$$

The Wien function approximates the Planck one well when the exponential term is larger than 1, which is true in the Wien limit $h\nu A^i(1-\mathbf{B}^i\cdot\mathbf{\Omega})/k \gg 1$ [61]. In addition, this function maximizes the Boltzmann entropy [27,28,61], which applies for neutrons as shown in [28]. Hence it is a good approximation for neutrons. For the sake of simplicity and without any further approximation, we rewrite the Wien function for a given bin as follows:

$$I_w^i = A_i(\nu)\exp(\nu\mathbf{B}_i\cdot\mathbf{\Omega}) \tag{18}$$

where A_i and $\mathbf{B}_i$ designate new dimensional quantities that have absorbed the universal constant coefficients: $A_i(\nu) = 2h\nu^3/c^2\exp(-h\nu A^i/k)$ and $\mathbf{B}_i = h/k\ A^i\mathbf{B}^i$. As explained above, in a bin framework, there is only one $A_i(\nu)$ and one $\mathbf{B}_i$ per bin, but in the limit of an infinite number of bins/frequencies, there is one $A_i(\nu)$ and one $\mathbf{B}_i$ per frequency, which should then be written $A_\nu(\nu)$ and $\mathbf{B}_\nu$.

It should be noted here that we are now in a very similar situation to [27,28], where the intensity (18) is used to derive a closure model for radiation [27] and neutron transport [28].

We now take angular moments of the function I^i_w (18) and use definitions (4)–(7) to obtain expressions for the angular moments $E^\nu_R, \mathbf{F}^\nu_R$, and $\mathbf{P}^\nu_R$ by direct integration. In doing so we approximate the integrals over $[\nu_{i_k} - \Delta\nu/2, \nu_{i_k} + \Delta\nu/2]$ by the midpoint rule to obtain equalities relating the integrands; this approximation will be used for all subsequent developments. The resulting equations are valid for all ν in bin i:

$$E^\nu_R = \frac{1}{c}\langle I^i_w\rangle_\Omega = 4\pi\frac{A_i(\nu)}{B_i\nu}\sinh(B_i\nu), \tag{19}$$

$$\mathbf{F}^\nu_R = \langle \mathbf{\Omega} I^i_w\rangle_\Omega = cE^\nu_R\frac{\mathbf{B}_i}{B_i}\left(\frac{\cosh(B_i\nu)}{\sinh(B_i\nu)} - \frac{1}{B_i\nu}\right) = cE^\nu_R\frac{\mathbf{B}_i}{B_i}\left(\frac{1}{\tanh(B_i\nu)} - \frac{1}{B_i\nu}\right), \tag{20}$$

and

$$\mathbf{P}^\nu_R = \frac{1}{c}\langle \mathbf{\Omega}\otimes\mathbf{\Omega} I^i_w\rangle_\Omega = E^\nu_R\left(\frac{1-\chi^\nu}{2}\mathbf{Id} + \frac{3\chi^\nu - 1}{2}\frac{\mathbf{f}^\nu\otimes\mathbf{f}^\nu}{f^{\nu 2}}\right), \tag{21}$$

where

$$\chi^\nu = 1 - 2\frac{F^\nu_R}{E^\nu_R B_i\nu} = 1 - 2\frac{f^\nu}{B_i\nu}, \tag{22}$$

in which $\mathbf{f}^\nu = \mathbf{F}^\nu_R/(cE^\nu_R)$ is the anisotropy factor for each wavelength, and the norm of a vector $\mathbf{v}$ has been denoted as v. We refer to [27,28,17] for the details of the integrations.

5.1. Closing B_i

Using Eq. (20), the norm of the flux is given by

$$F^\nu_R = cE^\nu_R\left(\frac{1}{\tanh(B_i\nu)} - \frac{1}{B_i\nu}\right). \tag{23}$$

It should be noted here that combining Eq. (20) and (23) leads without any approximation to

$$\frac{\mathbf{f}^\nu}{f^\nu} = \frac{\mathbf{B}_i}{B_i} \tag{24}$$

This result comes from the assumed form of the pseudo-intensity, (16) or (18), which requires that, inside bin i, there exists one $A_i(\nu)$ and one $\mathbf{B}_i$.

Summing over the ν's in the bin in Eq. (23), we obtain

$$\sum_{i_k}\frac{F^{\nu_{i_k}}_R}{cE^{\nu_{i_k}}_R} = \sum_{i_k}\left(\frac{1}{\tanh(B_i\nu_{i_k})} - \frac{1}{B_i\nu_{i_k}}\right). \tag{25}$$

We now assume that, within a bin

$$f^i = \frac{\sum_{i_k}F^{\nu_{i_k}}_R}{\sum_{i_k}cE^{\nu_{i_k}}_R} \simeq \frac{1}{N_i}\sum_{i_k}\frac{F^{\nu_{i_k}}_R}{cE^{\nu_{i_k}}_R} = \frac{1}{N_i}\sum_{i_k}f^{\nu_{i_k}}. \tag{26}$$

where N_i denotes the number of ν's in bin i. In other words we assume that the bin-value f^i is close to the average of the f^ν's: $f^i \simeq 1/N_i\sum_{i_k}f^{\nu_{i_k}}$. This approximation is exact for infinitely narrow bins or when f^ν is constant in a bin $\left(\text{since } f^i = \sum_{i_k}F^{\nu_{i_k}}_R/\sum_{i_k}cE^{\nu_{i_k}}_R = \sum_{i_k}cf^{\nu_{i_k}}E^{\nu_{i_k}}_R/\sum_{i_k}cE^{\nu_{i_k}}_R = f^{\nu_{i_k}}\right)$. In other cases Eq. (26) seems reasonable provided the bins are defined for fairly narrow ranges of opacity, such that the anisotropy does not vary too much in each bin (at a given position). This assumption will be tested numerically in Section 6.3. Using Eqs. (26), Eq. (25) becomes simply

$$f^i \simeq \frac{1}{N_i}\sum_{i_k}\frac{1}{\tanh(B_i\nu_{i_k})} - \frac{1}{N_i}\sum_{i_k}\frac{1}{B_i\nu_{i_k}}. \tag{27}$$

Eq. (27) will be called the closure equation. It is a *nonlinear scalar relationship* which gives the value of the scalar B_i for a given scalar f^i.

Similarly, the vector $\mathbf{B}_i$ is given by

$$\mathbf{f}^i \simeq \frac{\mathbf{B}_i}{B_i}\left(\frac{1}{N_i}\sum_{i_k}\frac{1}{\tanh(B_i v_{i_k})}-\frac{1}{N_i}\sum_{i_k}\frac{1}{B_i v_{i_k}}\right). \tag{28}$$

Eqs. (27) and (28) are closed so that for any given $\mathbf{f}^i$ a solution $\mathbf{B}_i$ of the system can be obtained. Since a closed-form solution cannot be derived, we use a Newton–Raphson algorithm to obtain $\mathbf{B}_i$.

The closure approximation Eq. (27) can be combined with Eq. (28) to obtain

$$\frac{\mathbf{f}^i}{f^i} \simeq \frac{\mathbf{B}_i}{B_i} \tag{29}$$

This important property will be used below.

5.2. Closing the pressure

Summing over the v's in bin i in Eq. (21) leads to

$$\mathbf{P}_R^i = \frac{1}{2}\left(\sum_{i_k}E_R^{v_{i_k}}-\sum_{i_k}E_R^{v_{i_k}}\chi^{v_{i_k}}\right)\mathbf{Id}+\frac{3}{2}\sum_{i_k}E_R^{v_{i_k}}\chi^{v_{i_k}}\frac{\mathbf{f}^{v_{i_k}}\otimes\mathbf{f}^{v_{i_k}}}{f^{v_{i_k}2}}-\frac{1}{2}\sum_{i_k}E_R^{v_{i_k}}\frac{\mathbf{f}^{v_{i_k}}\otimes\mathbf{f}^{v_{i_k}}}{f^{v_{i_k}2}}, \tag{30}$$

which can be written as

$$\mathbf{P}_R^i = E_R^i\left(\frac{1}{2}\left(1-\frac{\sum_{i_k}E_R^{v_{i_k}}\chi^{v_{i_k}}}{\sum_{i_k}E_R^{v_{i_k}}}\right)\mathbf{Id}+\frac{3}{2}\frac{\sum_{i_k}E_R^{v_{i_k}}\chi^{v_{i_k}}\frac{\mathbf{f}^{v_{i_k}}\otimes\mathbf{f}^{v_{i_k}}}{f^{v_{i_k}2}}}{\sum_{i_k}E_R^{v_{i_k}}}-\frac{1}{2}\frac{\sum_{i_k}E_R^{v_{i_k}}\frac{\mathbf{f}^{v_{i_k}}\otimes\mathbf{f}^{v_{i_k}}}{f^{v_{i_k}2}}}{\sum_{i_k}E_R^{v_{i_k}}}\right). \tag{31}$$

Using Eqs. (24) and (29), we obtain

$$\frac{\mathbf{f}^v\otimes\mathbf{f}^v}{f^{v2}}=\frac{\mathbf{B}_i\otimes\mathbf{B}_i}{B_i^2}\simeq\frac{\mathbf{f}^i\otimes\mathbf{f}^i}{f^{i2}} \tag{32}$$

Then, using Eq. (32), Eq. (31) becomes

$$\mathbf{P}_R^i = E_R^i\left(\frac{1}{2}\left(1-\frac{\sum_{i_k}E_R^{v_{i_k}}\chi^{v_{i_k}}}{\sum_{i_k}E_R^{v_{i_k}}}\right)\mathbf{Id}+\frac{3}{2}\left(\frac{\sum_{i_k}E_R^{v_{i_k}}\chi^{v_{i_k}}}{\sum_{i_k}E_R^{v_{i_k}}}-1\right)\frac{\mathbf{f}^i\otimes\mathbf{f}^i}{f^i}\right). \tag{33}$$

Then, defining $\chi^i=\sum_{i_k}E_R^{v_{i_k}}\chi^{v_{i_k}}/\sum_{i_k}E_R^{v_{i_k}}$, the pressure given in Eq. (33) is simply

$$\mathbf{P}_R^i = E_R^i\left(\left(\frac{1-\chi^i}{2}\right)\mathbf{Id}+\left(\frac{3\chi^i-1}{2}\right)\frac{\mathbf{f}^i\otimes\mathbf{f}^i}{f^i}\right). \tag{34}$$

We must now introduce a model for χ^i. Eq. (34) in 1D becomes $P_R^i=\chi^i E_R^i$. Similarly, using Eq. (21), we obtain $P_R^v=\chi^v E_R^v$. Hence, we have

$$\chi^i=\frac{P_R^i}{E_R^i}=\frac{\sum_{i_k}P_R^{v_{i_k}}}{\sum_{i_k}E_R^{v_{i_k}}}\quad\text{and}\quad\sum_{i_k}\chi^{v_{i_k}}=\sum_{i_k}\frac{P_R^{v_{i_k}}}{E^{v_{i_k}}}. \tag{35}$$

Previously, in Eq. (26), we have assumed that the binning should regroup the photons/neutrons of similar anisotropies. As a consequence, the averaged Eddington factor should be close to the bin value. Hence, we assume (similarly to Eq. (26)) that

$$\chi^i=\frac{\sum_{i_k}P_R^{v_{i_k}}}{\sum_{i_k}E_R^{v_{i_k}}}\simeq\frac{1}{N_i}\sum_{i_k}\frac{P_R^{v_{i_k}}}{E^i_{v_{i_k}}}=\frac{1}{N_i}\sum_{i_k}\chi^{v_{i_k}} \tag{36}$$

In Section 6.3, we will test numerically the assumption that the binning does regroup photons/neutrons such that χ^i is indeed close to $\frac{1}{N_i}\sum_{i_k}\chi^{\nu_{i_k}}$. Using the definition of χ^ν in Eq. (22), we obtain

$$\sum_{i_k}\chi^{\nu_{i_k}} = \sum_{i_k} 1 - 2\sum_{i_k}\frac{f^{\nu_{i_k}}}{B_i\nu_{i_k}} \tag{37}$$

Using (23), we have

$$\frac{f^\nu}{B_i\nu} = \frac{1}{B_i\nu}\left(\frac{1}{\tanh(B_i\nu)} - \frac{1}{B_i\nu}\right), \tag{38}$$

which when used in Eq. (37) leads to the approximation for χ^i:

$$\chi^i \simeq \frac{1}{N_i}\sum_{i_k}\chi^{\nu_{i_k}} = 1 - \frac{2}{N_i}\left(\sum_{i_k}\frac{1}{B_i\nu_{i_k}\tanh(B_i\nu_{i_k})} - \sum_{i_k}\frac{1}{(B_i\nu_{i_k})^2}\right). \tag{39}$$

The pressure model given in (34) with χ^i defined by (39) is closed since B_i is given from the anisotropy factor f^i through the relationship (27).

We have used only three assumptions to derive the by-bin moment model: the form of the underlying intensity (cf. Eq. (18)) and the approximations that the anisotropy and the Eddington factors in the bin are close to their respective bin-averages (cf. Eqs. (26) and (36)). These assumptions will be tested numerically in the next section. Eqs. (27), (39), and (34) define the by-bin pressure model. The multi-bin moment model is summarized in the following section.

5.3. Summary of the multi-bin model

The 3D multi-bin moment model we have developed is given by

$$\partial_t E_R^i + \nabla\cdot\mathbf{F}_R^i = c4\pi\bar{\sigma}_i S^i - c\bar{\sigma}_i E_R^i, \tag{40}$$

$$\frac{1}{c}\partial_t\mathbf{F}_R^i + c\nabla\cdot\mathbf{D}_R^i E_R^i = -\bar{\sigma}_i\mathbf{F}_R^i. \tag{41}$$

in which the multi-bin Eddington tensor $\mathbf{D}_R^i$ is given by

$$\mathbf{D}_R^i = \mathbf{P}_R^i/E_R^i = \left(\left(\frac{1-\chi^i}{2}\right)\mathbf{Id} + \left(\frac{3\chi^i-1}{2}\right)\frac{\mathbf{f}^i\otimes\mathbf{f}^i}{f^i}\right). \tag{42}$$

It is a function of the anisotropy $\mathbf{f}^i = \mathbf{F}_R^i/(cE_R^i)$ and the Eddington factor χ^i given by

$$\chi^i = 1 - \frac{2}{N_i}\left(\sum_{i_k}\frac{1}{B_i\nu_{i_k}\tanh(B_i\nu_{i_k})} - \sum_{i_k}\frac{1}{(B_i\nu_{i_k})^2}\right). \tag{43}$$

The scalar χ^i is defined in terms of the scalar B_i which is a solution of the following nonlinear scalar relationship for any given anisotropy norm $f^i = F_R^i/(cE_R^i)$:

$$f^i = \frac{1}{N_i}\sum_{i_k}\frac{1}{\tanh(B_i\nu_{i_k})} - \frac{1}{N_i}\sum_{i_k}\frac{1}{B_i\nu_{i_k}}. \tag{44}$$

Note that it could be possible to further simply the modeling but we do not recommend it; an analytical expression for B_i can be obtained from Eq. (44) if a Taylor expansion is performed for small anisotropy f^ν in Eq. (23). However, the resulting models for χ_i have not been found accurate, which is not surprising since $f^\nu \sim 0$ does not hold in our test cases.

For the numerical treatment of this system, the reader can refer to [65,22]. In [20,21,23,24,66], implicit formulations and preconditioning methods, which are usually mandatory for radiation-hydrodynamic problems, are presented.

5.4. Bin construction

In the following problems, we form the bins using a spatial average opacity as follows. The function $C(\nu)$ returns the bin number of frequency ν:

$$C(\nu) = 1 + \mathrm{floor}\left((n-1)\frac{\log(\bar{\sigma}_\nu) - \log(\bar{\sigma}_{\min})}{\log(\bar{\sigma}_{\max}) - \log(\bar{\sigma}_{\min})} + 0.5 \right), \tag{45}$$

where the function floor(x) returns the greatest integer value less than or equal to x, $\bar{\sigma}_\nu$ is the spatial average of $\sigma(\nu)$, and $\bar{\sigma}_{\max}$ and $\bar{\sigma}_{\min}$ are its maximum and minimum values. n is the total number of bins.

Such a binning should be effective for spatially constant opacity, but, as we will see in the next section, it is far from being optimal in the variable case.[4] It creates in fact unoccupied bins for some radii. On the other hand, it is conceptually easy and of low numerical cost to bin using the function C. As a result, the creation of the source terms, mean absorption coefficients, and closure terms is neither difficult nor very costly. In addition, since such a binning does not depend on the radius (because mean opacities are used) the system of Eqs. (40) and (41) does not contain boundary terms due to the non-commutation of spatial differentiation and bin integrals.

Many criteria can be chosen to define bins. For instance, the pickets (bin-dividing opacities) have been chosen so that the ratio between successive values is roughly the same in [45]. Another example is in [53], and references in it, where the binning of solar atmospheres is explained. Particular care is needed for this process in order to minimize the number of bins while accounting for most of the physics to obtain good accuracy. As pointed out in the introduction, many other binning methods of much more sophisticated forms have been proposed, but complexities arise in these cases. For instance, when a method introduces a PDF in the re-arrangement/averaging procedure, it should be checked that the PDF does not need to be also included in the closure model in order to be mathematically consistent.

5.5. On a general multi-band formulation

The closure has been derived for a set of frequencies which we have assumed to be representative of the whole spectrum. However this is not mandatory. The derivation is unchanged if we would have accounted for frequencies inside a group, like in the ODF or multi-band methods [3]. It is hence possible to solve Eqs. (40) and (41) for each bin inside given groups. The sum of moments of the bins will give the moment in a given group and the sum of the moments of all groups will provide the moment on the whole spectrum. The advantage is that the propagation is always solved in the bin, which, we claim, is a guarantee of better accuracy. Eqs. (40) and (41) describe thus a general multi-band moment method, but for which the binning has not been assumed spatially dependent. However, if one uses a large number of groups such that there are not many frequencies left for the binning, then the hypotheses used in the derivation would not been satisfied and the model accuracy would be degraded. A division by group may separate opacities of the same order of magnitude into different groups, leading to inefficiency. There is thus a trade-off between the number of groups and the number of bins. We believe the best accuracy is likely to be obtained when a small number of frequency groups are defined, following for instance a grouping into X-rays, EUV, UV, V, IR, and MW, leaving inside each of them many frequencies to be binned together. That way one also gets access to by-group quantities, like the flux in the IR or the optical emitted power in the visible, etc., which can be very important for engineering purposes.

We note that the problem of non-commutation of operators, coming from the re-arrangement of the opacity and which we avoid here by only considering either spatially constant opacities or a mean-opacity binning, is common to any multi-band formulation and is not a result of using moment methods. This problem should be handled as it is in other methods, such as DOM or as explained in [56].

[4] In particular in the solar case, where large variations of the opacity occur along the radius.

6. Numerical results

6.1. Radiation in a spherical solar atmosphere

We wish first to assess the accuracy of the closure for χ^i given by (43) and (44) without the approximation of using a moment method. To do this, we use an RTE solver to obtain an accurate intensity and then use this intensity to compute $E^i_R, \mathbf{F}^i_R$, and $\mathbf{P}^i_R$ using Eqs. (4)–(7). The exact values of the Eddington tensor are then $\mathbf{P}^i_R/E^i_R$. The model χ^i is evaluated from (43) and (44) using these same E^i_R and $\mathbf{F}^i_R$. This technique has been fully explained and used in [18] (where the same code is used to obtain the intensity). This method allows us to determine if the closure expression is accurate and, since in the moment approach the closure constitutes the crucial approximation, gives information on the accuracy that can be expected from it.

In this section, we will focus on demonstrating the validity of the assumptions used to derive the closure and on its accuracy. We will show that the non-linearity of the closure is trivial to solve, which leads to a readily computable model, and we will assess the closure performance on a complex test case of interest: the solar atmosphere. We will also compare our closure with the P_1 one, i.e. $\chi^i = 1/3$ for every r, ν, and bin. We believe that a solid theoretical and numerical demonstration of the validity and usability of the closure will give confidence to those willing to use the systems (12)–(15).

The temperature and opacity profiles of our spherically symmetric solar atmosphere are shown in Figs. 1 and 2 respectively. The domain starts from below the visible surface (a very opaque region), passes through the surface (located between $r = 696{,}000$ km and 696,050 km), and ends at 600 km altitude, in the solar chromosphere. These profiles have been provided by Stein and Nordlund [48,50,51,49,52]. We also plot in these figures the radiative temperature $T_R = (E_R/a)^{1/4}$ and the radiative source term $\mathrm{div}(\mathbf{F}_R)$ obtained by solving the RTE for 2748 frequencies. We use a ray-tracing code written for a spherically symmetric configuration [18]. The source term profile shown in Fig. 1 is very typical of the solar atmosphere. Inside the sun, emission compensates absorption (giving radiative equilibrium, $\mathrm{div}(\mathbf{F}_R) \simeq 0$). At the surface, a strong cooling by radiation occurs due to strong emission, $\mathrm{div}(\mathbf{F}_R) \gg 0$. In the lower chromosphere, absorption occurs (the absorption peak is at $r = 696{,}100$ km).

Fig. 3 (left) and (right) shows the percent error of the closure model for different numbers of bins.[5] This error is integrated over all bins or frequencies. In the case where there are as many bins as frequencies (curve annotated with crosses), the error reaches a peak of 10% just above the surface and is bounded by 5% in the chromosphere. These results are very good and demonstrate the validity of a Wien function to close the system. In the case where there are as many bins as frequencies, this is the only assumption used in the derivation. For low numbers of bins $n = 8, 10, 15$, the peak of error is around 12% and the error is bounded by 10% in the chromosphere. The maximal error is reached for the case of one single bin which is the gray case; it confirms the non-gray character of this atmosphere.

These results show that the bin closure is accurate. However, these results must be tempered by two remarks: first, due to the particular choice of the binning, many bins are unoccupied. This means than even fewer occupied bins are needed to reach a certain accuracy. By definition, we consider a bin to be occupied if it contains a reasonable fraction of the total number of frequencies and if the total intensity in those frequencies is not negligible; otherwise we call it unoccupied. Because some bins are unoccupied the percent error is effectively lowered. Hence these results must be complemented by measuring the error in each bin or frequency. This will be done in the following paragraphs.

6.1.1. Infinitely narrow bins

Until otherwise noted, the x-axis represents the solar radius in kilometers and the wavelengths are given in Angstroms. The names of the quantities plotted in the figures are given in the captions along with their units.

6.1.1.1. We first test our model using one bin per frequency to see in isolation the accuracy of the closure, to validate the Wien form of the intensity, and to be able to see afterward the loss of accuracy due to binning.

[5] The percent error is the difference between the model and exact expressions as a percentage of the exact one.

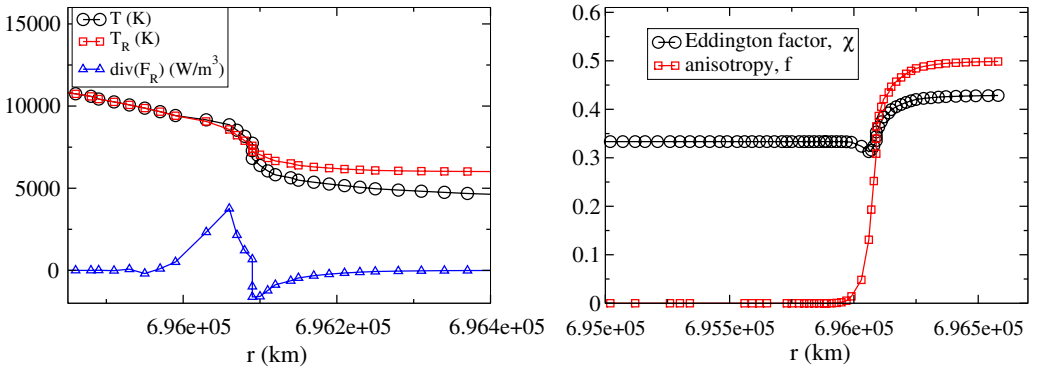

Fig. 1. Solar atmosphere. (Left) temperature (K), radiative temperature ($T_R = (E_R/a)^{1/4}$ in K), and radiative source term in W/m^{-3}. (Right) ν-integrated anisotropy and Eddington factor.

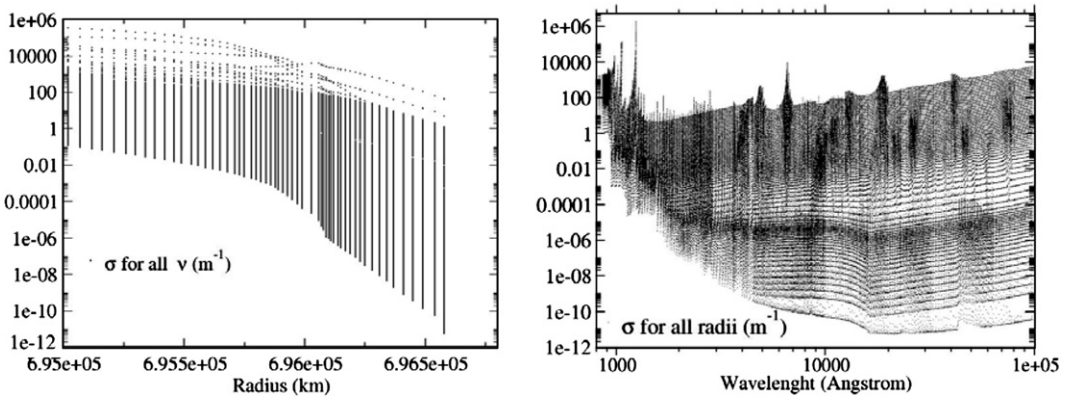

Fig. 2. (Left) opacity values $\sigma(\nu)$ for 2748 ν's. (Right) $\sigma(\nu)$ for all radii.

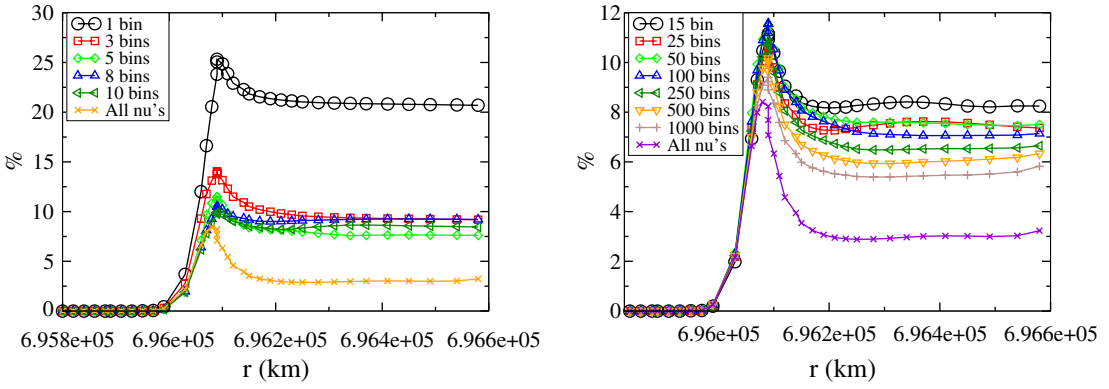

Fig. 3. Sun with all ν's. ν-integrated error of the pressure model for different binnings.

Fig. 4: the exact (left) and modeled (right) Eddington factors are shown for each of the 2748 frequencies. They are found to be very similar. Fig. 5 shows the percent error (for a clear comparison) of our closure and of P_1. Our model has an error bounded by 22%. The large errors (from 15% to 22%) occur right at the surface and in the absorption region, i.e. for $r \in [696050, 696150]$ km where the model, instead of staying at equilibrium, i.e.

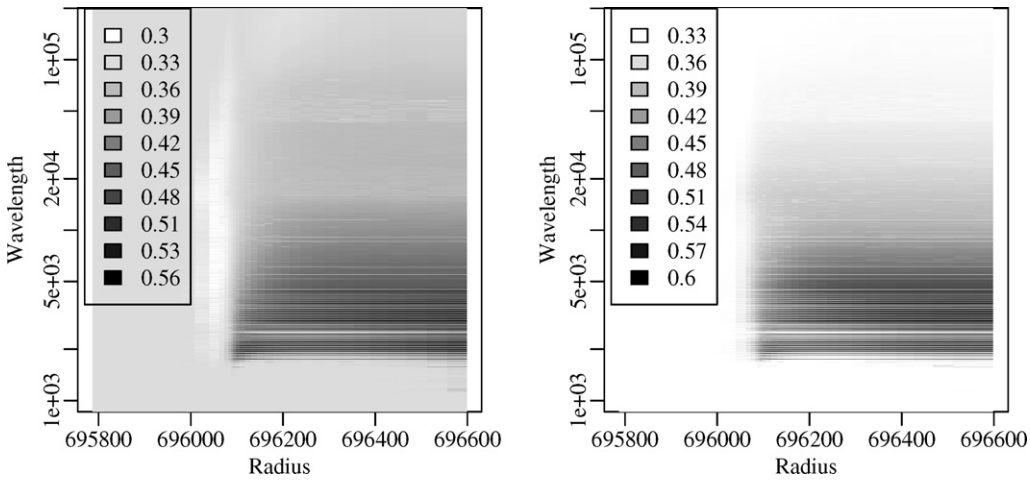

Fig. 4. Sun with all ν's. Exact (left) and modeled (right) Eddington factor.

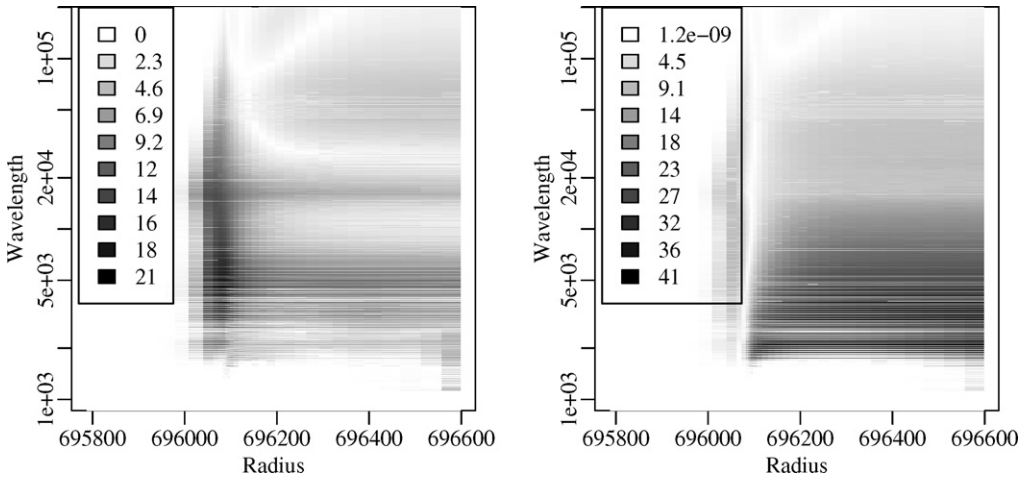

Fig. 5. Sun with all ν's. Error of the modeled Eddington tensor (left) and of P_1 (right).

$\chi = 1/3$, incorrectly perceives some anisotropy and raises χ up to 0.4. The exact Eddington tensor goes slightly below 1/3 (the minimal value is 0.3 in the absorption region). We believe this error is acceptable since at slightly higher radii the errors are below 15% at worst and mostly below 10%.[6] The comparison with P_1 in Fig. 5 (right), where $\chi = 1/3$, shows a clear improvement brought by our modeling. Fig. 6 shows the radiative energy and fluxes: the radiation is concentrated below 20000 Å. The dominant part is below 5000 Å. Now, reconsidering the closure model, it can be seen that below 5000 Å, the model is accurate with a peak error around 12–15% and around 5% in the chromosphere. The anisotropy, Fig. 6 (right), is however not too high, mostly around 0.5–0.6, so we also tested the model on a higher anisotropy case (cf. following subsection).

6.1.1.2. On the P_1 closure. Looking again at Fig. 1 (right), one could conclude, looking at only ν-integrated quantities, that since the Eddington factor of this solar atmosphere is between 0.3 and 0.45, P_1, which models this term by 1/3, is usable. This would be wrong, as we can see by looking at the by-bin quantities. Fig. 6 (left) and (center) shows radiative cooling occuring for wavelengths $\lambda \in [2000, 10{,}000]$ Å. In this region, the error

[6] See also in Fig. 3 for the integrated error.

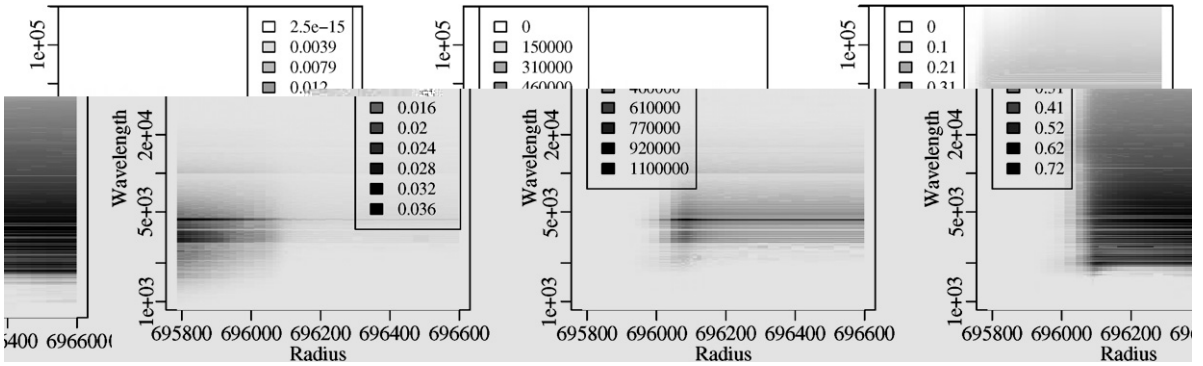

Fig. 6. Sun with all ν's. Moments: E_R^ν in W/m^{-3} s^{-1} (left), F_R^ν in W/m^{-2} (center), and anisotrpy f^ν (right).

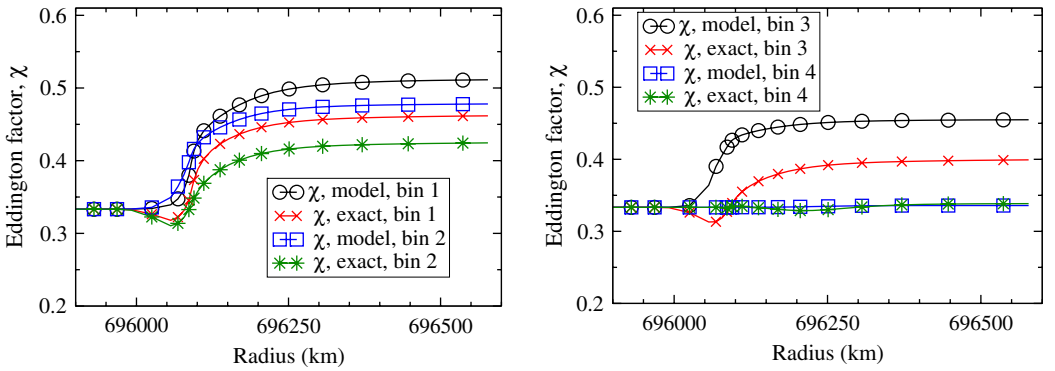

Fig. 7. Sun with three occupied bins. Exact and modeled Eddington factor.

committed by the P_1 closure (Fig. 5 (left)) goes from 20% to 30% for $\lambda \in [5000, 10000]$ Å and from 30% to 40% for $\lambda \in [2000, 5000]$ Å, where radiation is dominant. The latter corresponds to anisotropic Eddington factor values around 0.6, which are approximated by an isotropic value of 0.33. This explains why P_1 will overestimate the cooling by radiation when used in computations of the solar atmosphere. It also reminds one to look at non-ν-integrated quantities.

6.1.2. 3, 10, 21 Occupied bins

In this subsection, we test the closure using 5, 15, and 40 bins. The binning is done according to Eq. (45). Low and high bin numbers represent respectively low and high mean-opacity values. As stated, the simple binning method retained here is far from being optimal (in particular for opacities varying in space). As a result many bins are unoccupied or contain just a few frequencies. In fact, we are actually treating cases of 3, 10, and 21 *occupied* bins and have thus chosen to refer to the cases as 3, 10, 21,[7] but we also plot the solution for some of the lightly occupied bins to assess the model's behavior in such cases and to show that it is not singular.

6.1.2.1. Three occupied bins. Fig. 7 shows the closure model results compared to the exact ones when three occupied bins are used. The model is unable to go under $\chi = 1/3$ (this shortcoming is inherent to moment models and is not a function of the number of bins). Its error is maximal close to the sun's surface, where the radiation leaves equilibrium. The model is more accurate for nearly transparent bins, which is a surprising and helpful property: we can presume that for hot sources radiating into cold media, the fluxes will be correctly

[7] Contrary to the nomenclature used in Figs. 3 and 16.

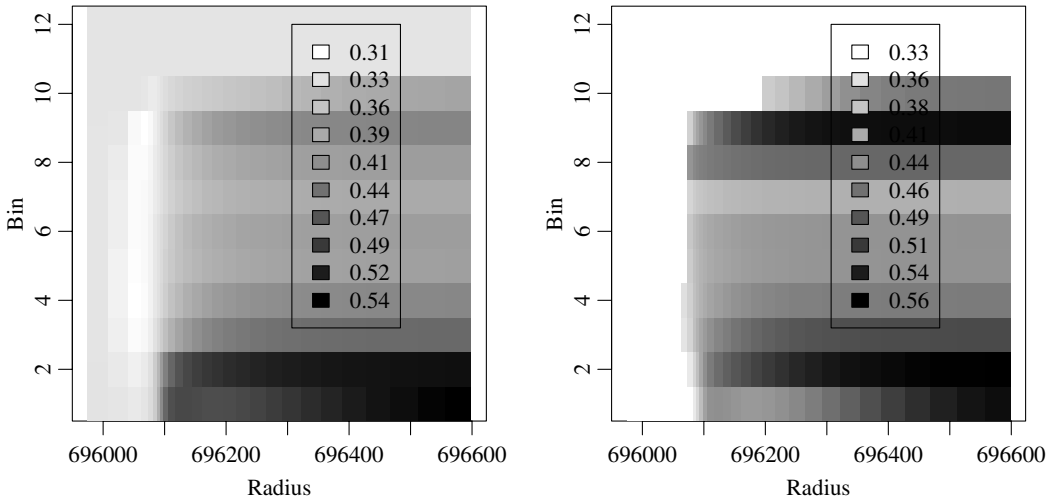

Fig. 8. Sun with 10 occupied bins. Exact (left) and modeled (right) Eddington factor.

limited. Even though the correct trends are computed, poor accuracy of the model is evident, indicating that more bins are needed.

6.1.2.2. Ten occupied bins. Fig. 8 shows the model and exact closure model results for the 10 occupied bins case.[8] Fig. 9 (left) quantifies the comparison by showing the percent error. The model is found to be accurate for the seven first bins. For those bins, the maximum loss of accuracy occurs close to the surface at exactly $r = 696{,}100$ km (the region of strong absorption) and is around 15% due to an overestimation of χ Fig. 10.[9] The accuracy is between 5% and 10% in the atmosphere and gives confidence of obtaining correctly limited fluxes. However the model has very poor accuracy for bins 8–10. This fortunately does not matter as those bins do not emit significant radiation: the plots of both radiative energy and fluxes in Fig. 10 (left-center) attest that radiation is concentrated in bins 1–6, where the model is very accurate. In addition, bins 8–10 do not contain many frequencies (see Fig. 11 (center)). Those poor results (bin 8–10) are simply due to our rough binning and do not represent a failure of the method. In contrast, the P_1 closure is very inaccurate, particularly for the low bin numbers (1–4) where accuracy matters the most (see Fig. 9 (right)). The plots of the moments (Fig. 10 (left-center)) also show that this atmosphere could be successfully solved by only considering those six occupied bins. Since the closure is found to be pretty accurate, the full moment solution is expected to be accurate.

In Fig. 11 (left), the logarithm of the number of iterations needed for the Newton algorithm when solving Eq. (27) is plotted. Very few iterations are needed (<10 at most radii[10]), and this number increases only close to equilibrium, where the solution is known (i.e. $\chi^i = 1/3$) and hence does not need to be computed. The negative values of the logarithm correspond to 0 iterations. These results show that there is no difficulty and no great numerical cost in solving Eq. (13).

6.1.2.3. Twenty-one occupied bins. Our next case considers 40 bins of which only 21 are occupied (see Fig. 11 (right)). According to the plots of the moments in Fig. 14 (left-center), it can be seen that radiation is concentrated from the first to the fifteenth bins. For those bins, looking carefully at both model and exact closures, we see that the model values are slight overestimates, but overall good agreement is observed (Fig. 12). The plot of the percent error in Fig. 13 (left) confirms that the error is very low. The improvement compared to P_1 is again confirmed in Fig. 13 (right). As in the cases with fewer bins, the model has poor accuracy in lightly

[8] See Fig. 11 (center) to see the number of v's per bin.

[9] This can be corrected easily by adding an *ad hoc* condition such as $\chi^i = 1/3$ *if* $f^i < 0.1$ *or* 0.2; see f^i plotted in Fig. 10 (right). Note also the accuracy of P_1 just at $r = 696100$.

[10] With a convergence criterion of 10^{-4}.

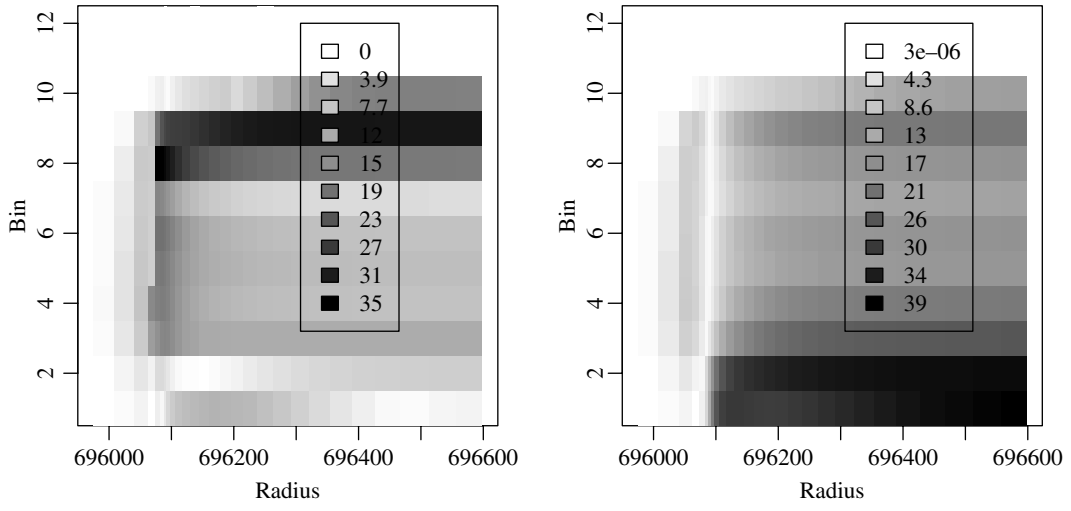

Fig. 9. Sun with 10 occupied bins. Error of the Eddington tensor: current model (left) and P_1 (right).

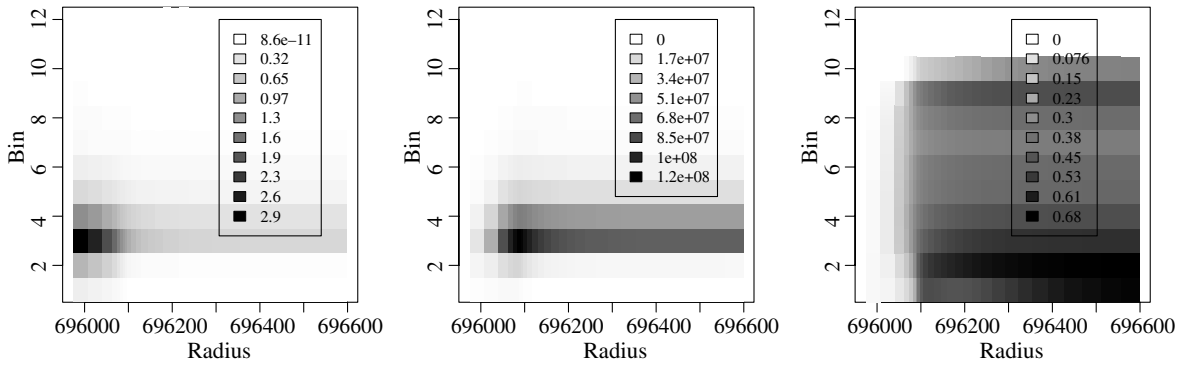

Fig. 10. Sun with 10 occupied bins. Moments: E_R^i in W/m^{-3} s^{-1} (left), F_R^i in W/m^{-2} (center), and anisotrpy f^i (right).

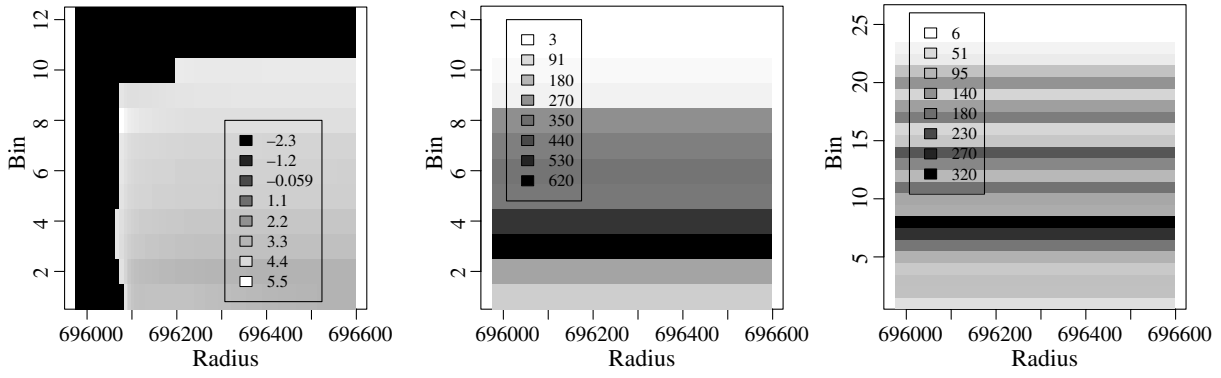

Fig. 11. log(N_{Newton}) (left) and number of v in a bin (center) for the sun with 10 occupied bins. Number of v in a bin for the sun with 21 occupied bins (right).

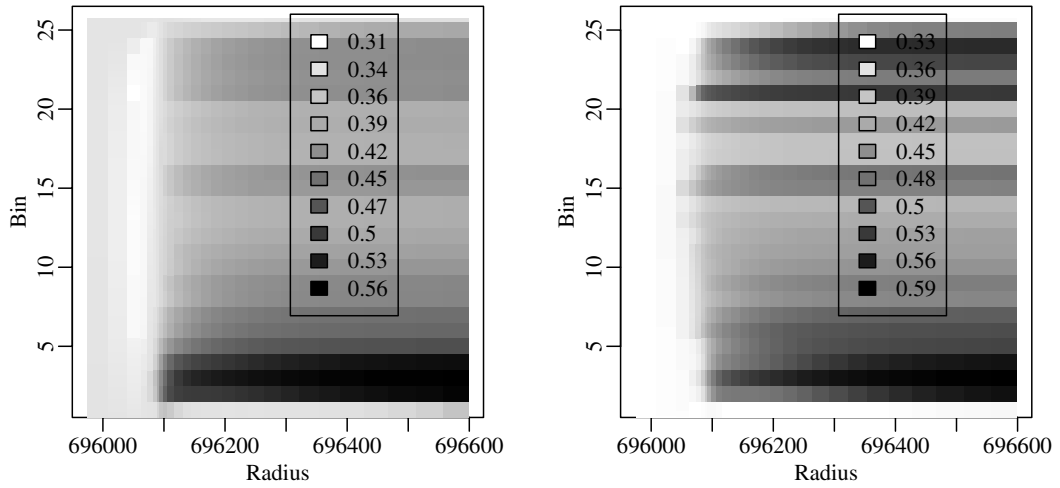

Fig. 12. Sun with 21 occupied bins. Exact (left) and modeled (right) Eddington factor.

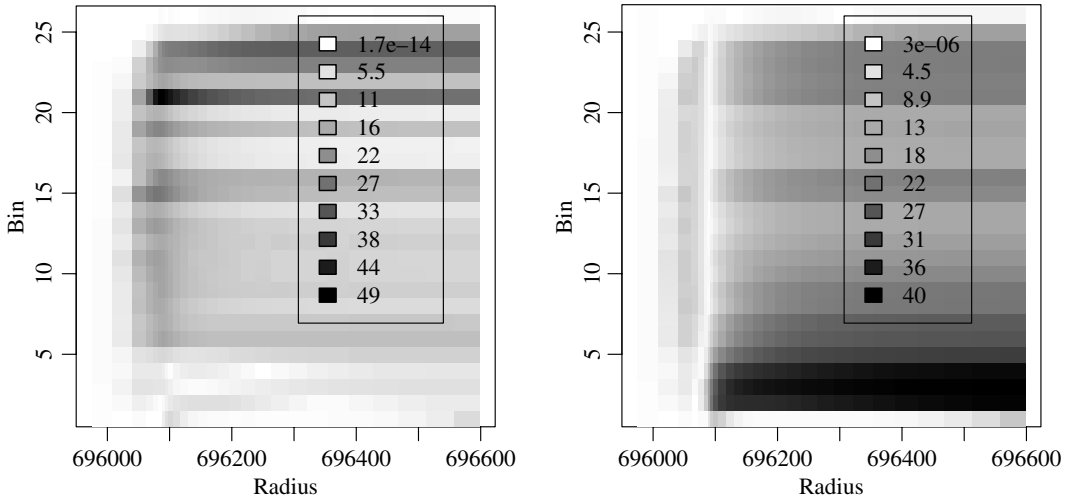

Fig. 13. Sun with 21 occupied bins. Error of the Eddington tensor: present model (left) and P_1 (right).

occupied bins and in those where the radiation is weak ($i > 15$), a fact we have not explained but which is inconsequential. It is clear that increasing the number of occupied bins from 10 to 21 improves the accuracy (as was seen in Fig. 3), in particular in the absorption zone. We also find that the number of Newton iterations remains as low as the 10 bins case.

6.2. Radiation in a artificial spherical atmosphere

In this section, we consider the case of an artificial atmosphere (noted AA in the figures) in order to increase the overall radiative anisotropy and to create a very challenging test for our model. To do this, we simply decreased the radius of the solar atmosphere by a large factor. The x-axis of the following figures represents the radius of the artificial atmosphere in meters and the wavelength is given in Angstroms. In Fig. 15 (right), the absolute value of the radiative source term is plotted: the first peak for $r \in [18, 22]$ km corresponds to a

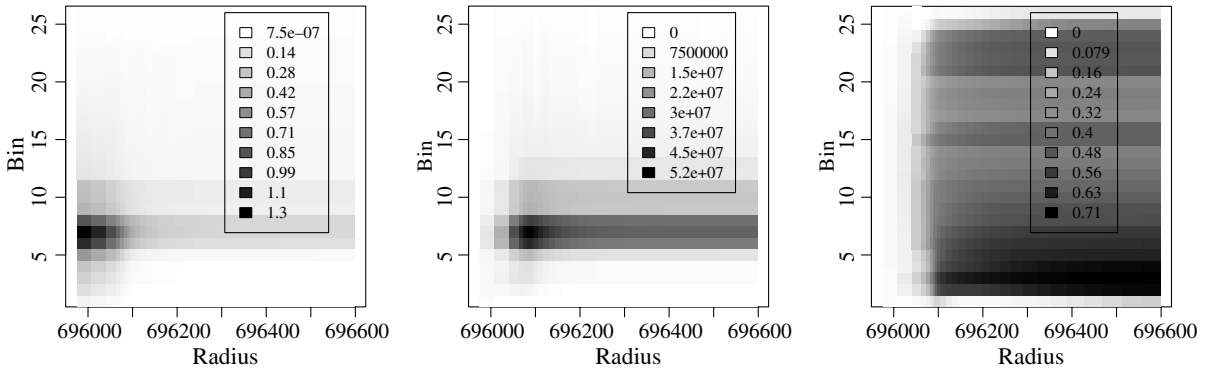

Fig. 14. Sun with 21 occupied bins. Moments: E_R^i in W/m^{-3} s^{-1} (left), F_R^i in W/m^{-2} (center), and anisotropy f^i (right).

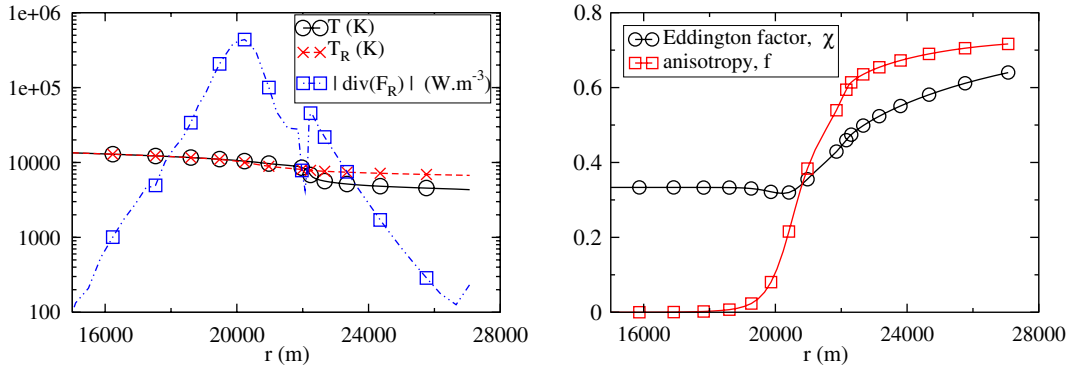

Fig. 15. AA. Left: logarithmic plot of the temperature (K), radiative temperature ($T_R = (E_R/a)^{1/4}$ in K), and the absolute value of the radiative source term in W/m^{-3}. Right: ν-integrated anisotropy and Eddington factor.

strong emission zone (much stronger than in the solar case). The second peak for $r \in [22, 23.5]$ km corresponds to an absorption zone. In Fig. 15 (left), we plot the integrated anisotropy and Eddington factor; these can be compared with Fig. 1 (left). For the solar case, the integrated Eddington factor is bounded above by 0.45 and the anisotropy by 0.5, which is not a very anisotropic average.[11] Reducing the radius of our new star to roughly 20 km and its atmosphere to roughly 7 km, we produce a higher average anisotropy, leading to an increased Eddington factor reaching 0.7. Even though this might not seem very anisotropic, we can see in Fig. 6 (left) that it leads, for certain wavelengths, to strong radiation propagating with a anisotropy f^ν between 0.8 and 0.9. We thus have created much more anisotropic radiation, in particular for wavelengths below 5000 Å. Comparing the f^ν's for the sun plotted in Fig. 6 (left) and those of the artificial atmosphere plotted in Fig. 19 (left) confirms this.

The plot of the integrated percent error of the closure model in Fig. 16 shows that the model becomes accurate in average starting from five bins (with errors <15%). As before, we should note that many bins are unoccupied, and these results need to be scrutinized. We will see below in detail that, as for the sun, an acceptable accuracy, i.e. a peak error between 10% and 15% in critical zones and an error contained mostly between 5% and 10% outside, occurs when 5–10 bins are fully occupied. Looking at the plots of the error obtained from all ν's (curve with crosses) we see that the error is here bounded by 12%, but is higher than in the sun case. We are unable to explain why the error increases as the number of bins increases in the far outer atmosphere. As for the solar case, we complement below these results by a finer analysis for each frequency.

[11] It should be noted that there is stronger anisotropy at some wavelengths (with $f^\nu \simeq 0.7$) participating in the cooling.

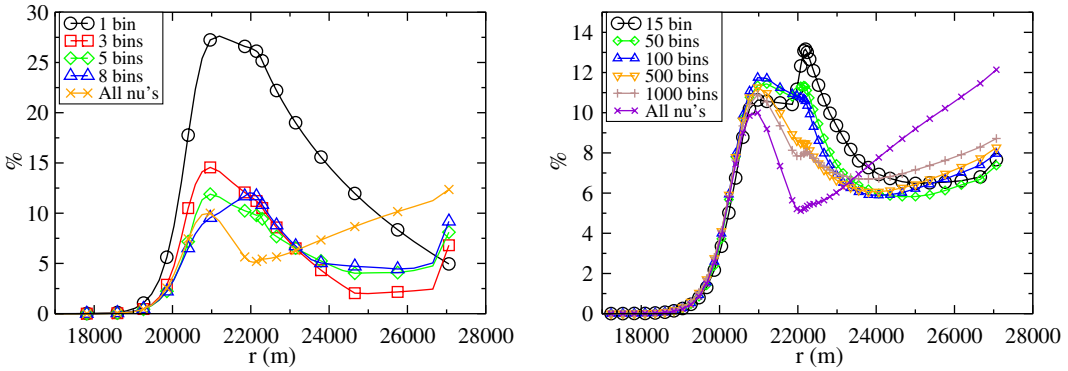

Fig. 16. AA with all ν's. ν-integrated error of the Eddington factor for different binnings.

6.2.1. Infinitely narrow bins

Fig. 17 shows the exact and modeled Eddington factor; we find again that the model captures most of the complexity of this term. Fig. 18 shows the percent error for our model (left) and for P_1 (right). Before analyzing these results, we must refer to Fig. 19 (left-center) where the moments are plotted. It can be seen that radiation is important for $\lambda \in [2000, 20{,}000]$ Å and is very strong for $\lambda \in [2000, 10{,}000]$ Å. First, for $\lambda \in [2000, 10{,}00]$ Å, the *large* error of the closure model, from 15% to 20% occurs around $r = 21$ km, where the radiative fluxes are maximal and emission is dominant. In this region, the value given by the model is too high: the approximate 1/3 value is overestimated by 20%, i.e. 0.4 instead of 0.3. We have here a case in which the emission is 200 times higher than in the solar case (10^6 W/m^3 instead of 5000 W/m^3) (cf. Figs. 1 and 15). In the absorption region, around 22 km, the error is mostly between 10% and 15%, as in the sun case. In the outer atmosphere the error is low, around 5% to 10%. This indicates that, for those wavelengths, the closure model, when used in a moment model, will correctly propagate the fluxes when they are strong. Fig. 19 (center) confirms that it is in this region ($r > 21$ km) that fluxes are dominant. Second, for $\lambda \in [10{,}000, 20{,}000]$ Å, our comments are similar, but we notice in addition a 20% error zone for $r \in [25, 27]$ km which we cannot explain.

Overall these results are poorer than in the sun case, confirming that this case is more challenging. However, we still consider that they demonstrate the accuracy of the closure. In comparison, P_1 is mostly wrong with errors between 50 and 60% for $\lambda \in [2000, 20{,}000]$ Å and $r > 21$ km, i.e. in regions where radiation is concentrated.

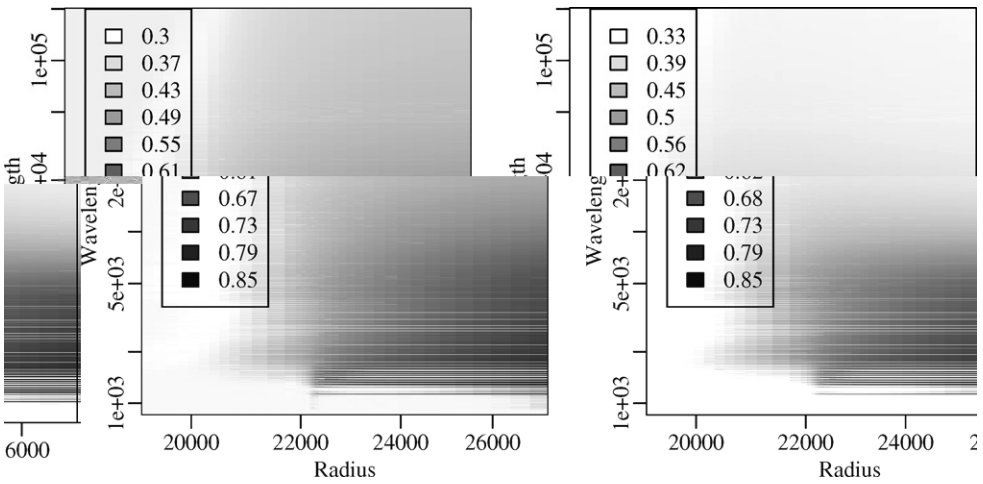

Fig. 17. AA with all ν's. Exact (left) and modeled (right) Eddington factor.

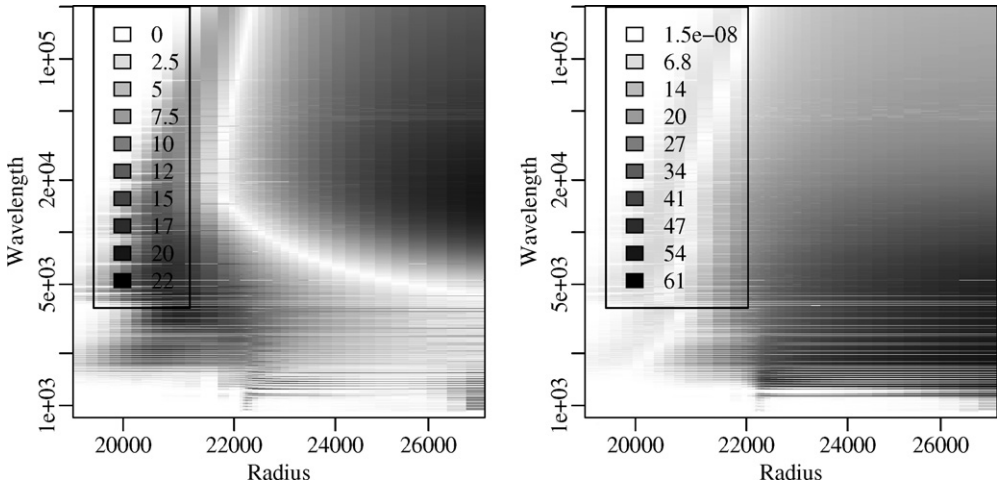

Fig. 18. AA with all ν's. Error of the Eddington factor: present model (left) and P_1 (right).

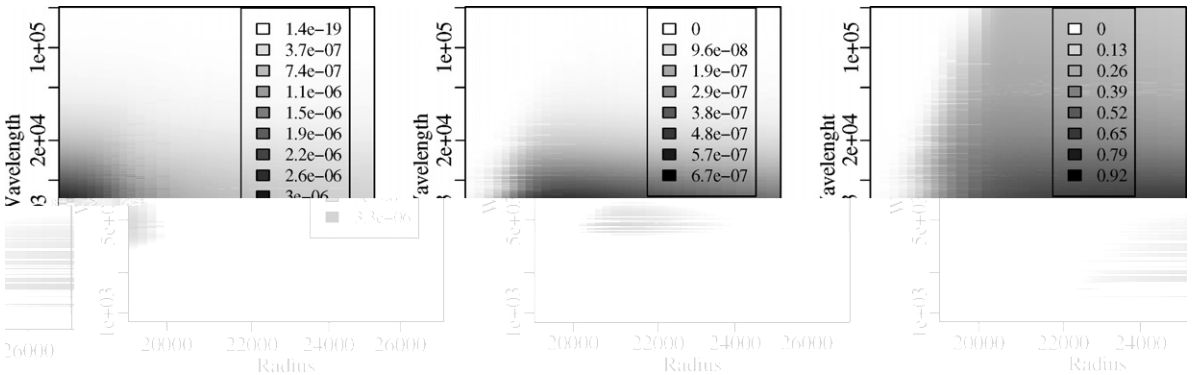

Fig. 19. AA with all ν's. Moments: E_R^ν in W/m^{-3} s^{-1} (left), F_R^ν in W/m^{-2} (center), and anisotrpy f^ν (right).

6.2.2. Twenty-one occupied bins

We now focus on the effect of the binning on the accuracy of the closure model. We consider 40 bins, but only 21 are occupied and representative. The case of 3 and 10 bins are not presented here but the same conclusions can be drawn. Fig. 20 shows the exact and modeled closures. For bins numbered lower than 16, they agree well. The plot of the moments in Fig. 22 indicates that radiation occurs for bins numbered lower than 15, with strong radiation from bin 5 to bin 8 (see also Fig. 23 (right)). The percent error plotted in Fig. 21 shows that the model is accurate for bins numbered lower than 16 (<5%, 10%, 15% error). Fig. 21 also shows an obvious improvement compared to P_1. The *large* 15–20% error occurs around $r = 21$ km, where the model value rises to around 0.4 instead of staying close to 1/3. This is the main critic, but, as previously mentioned, this can easily be corrected, and should have no major repercussions. Fig. 23 confirms that a small number of Newton iterations is needed (left) and indicates how the bins are occupied (right).

In Fig. 23 (center), looking at the logarithm of the dimensionless quantity $B_i(1/N_i)\sum_{i_k} \nu_{i_k}$, it can be seen that the behavior of B_i, solution of Eq. (27), is not simple, making the iterative solving of Eq. (27) unavoidable.

6.3. Testing the two mathematical assumptions

We have demonstrated in the previous Sections 6.1.1 and 6.2.1 that the choice of a Wien intensity to close the system is reasonable. This section is devoted to the direct testing of the two remaining approximations Eqs. (26) and (36): $f^i \simeq 1/N_i \sum_{i_k} f^{\nu_{i_k}}$ and $\chi^i \simeq 1/N_i \sum_{i_k} \chi^{\nu_{i_k}}$.

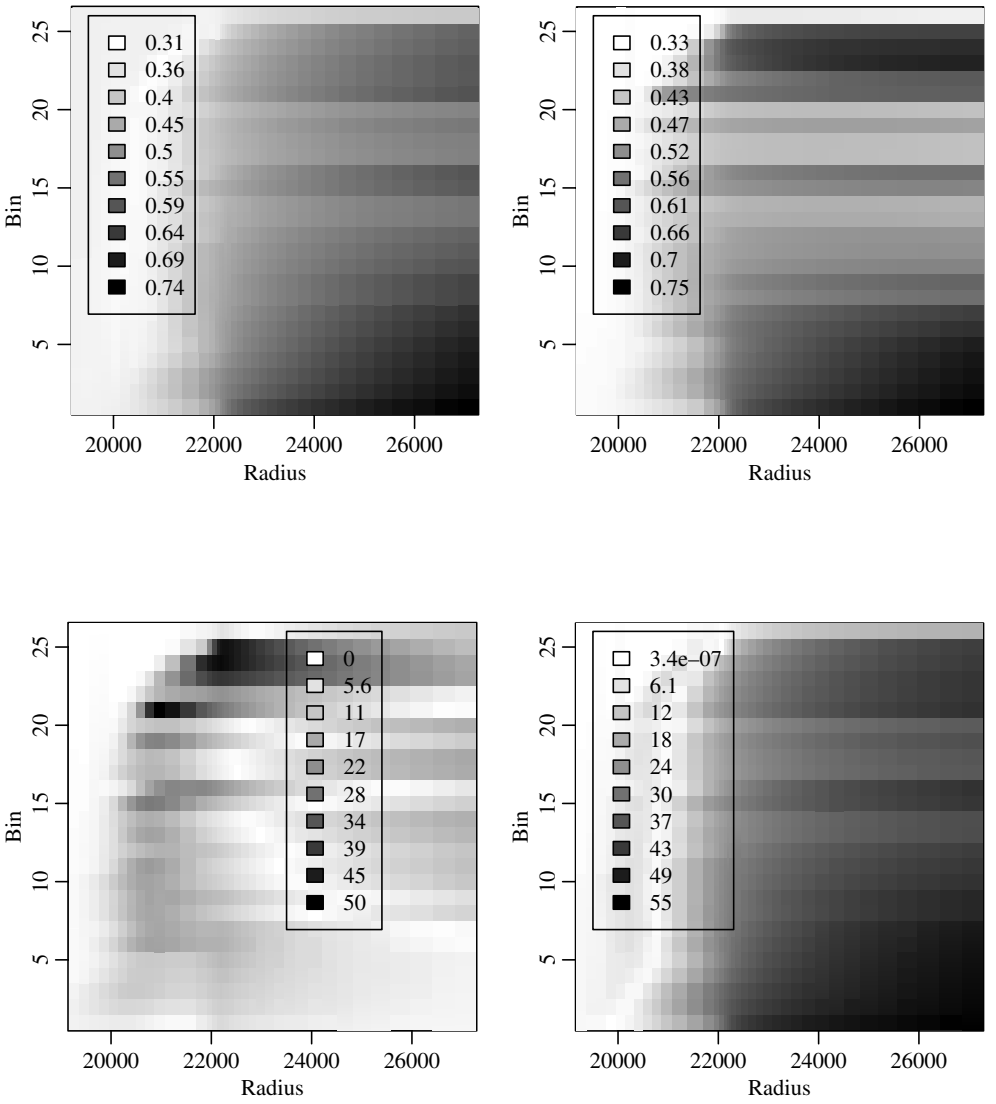

Fig. 21. AA with 21 occupied bins. Error of the Eddington tensor: current model (left) and P_1 (right).

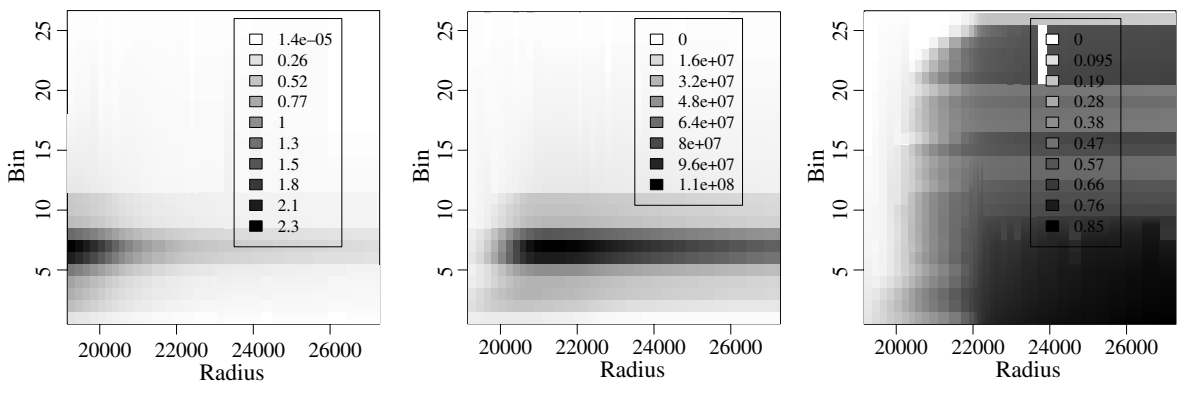

Fig. 22. AA with 21 occupied bins. Radiative energy in $W/m^{-3}\,s^{-1}$ (left), flux in W/m^{-2} (center), and anisotropy (right).

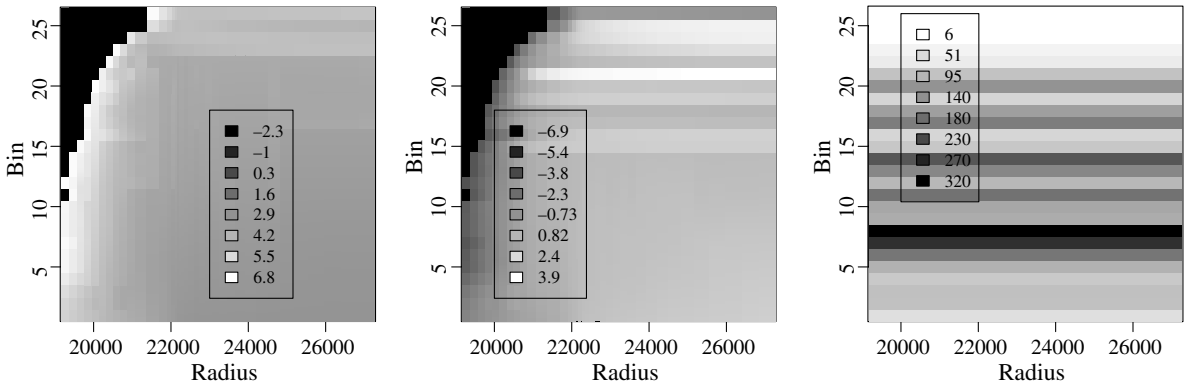

Fig. 23. AA with 21 occupied bins. (Left) $\log(N_{\text{Newton}})$. Center: $\log\left(B_i(1/N_i)\sum_{i_k} v_{i_k}\right)$. (Right) number of v in a bin.

We consider the two previous cases of 21 occupied bins for the solar atmosphere (Fig. 24) and the artificial atmosphere (Fig. 25). The x-axis represents the radial direction. The notation of superscript $b = 5, 6, \ldots$, etc. in the key means bin $i = 5, 6, \ldots$. We plot the anisotropies in the two left columns and the Eddington factors in the two right columns in each of these figures for the bins in which radiation is strong, i.e. bins $i = 5$ to $i = 10$ (cf. Figs. 14 and 22). In each of the sub-figures in the left columns we plot the f^v's for all v's in these bins (small circles), the bin value of the anisotropy in the bin i, i.e. $f^i = \sum_{i_k} F_R^{v_{i_k}} / \left(c \sum_{i_k} E_R^{v_{i_k}}\right)$ (plain curve), and the average anisotropy $f^{\text{av}} = 1/N_i \sum_{i_k} f^{v_{i_k}}$ (curve with large circles). Comparing the plain curve with the curve annotated with large circles gives the accuracy of the approximation made in Eq. (26). Similarly, in the two right columns

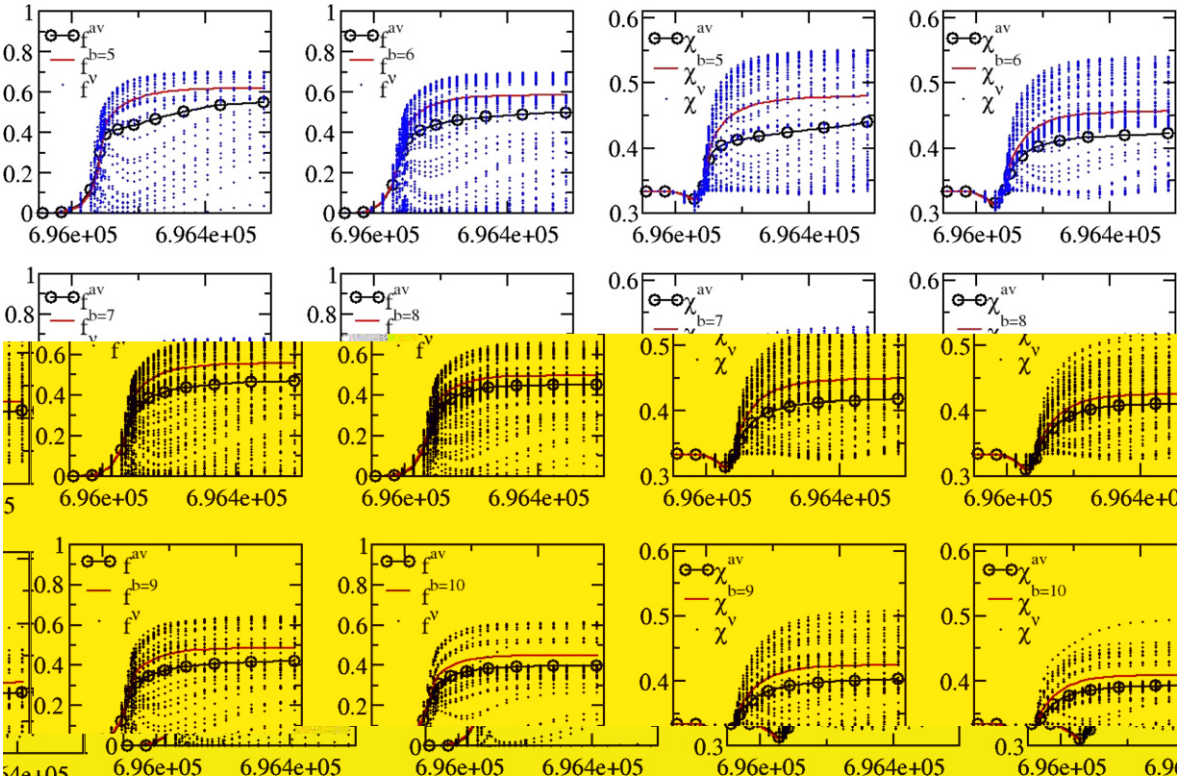

Fig. 24. Sun with 21 occupied bins. Plots of the v-values, the bin value, and the average v-value of the anisotropy (two columns on the left) and the Eddington factor (2 columns on the right) for bin numbers 5–10.

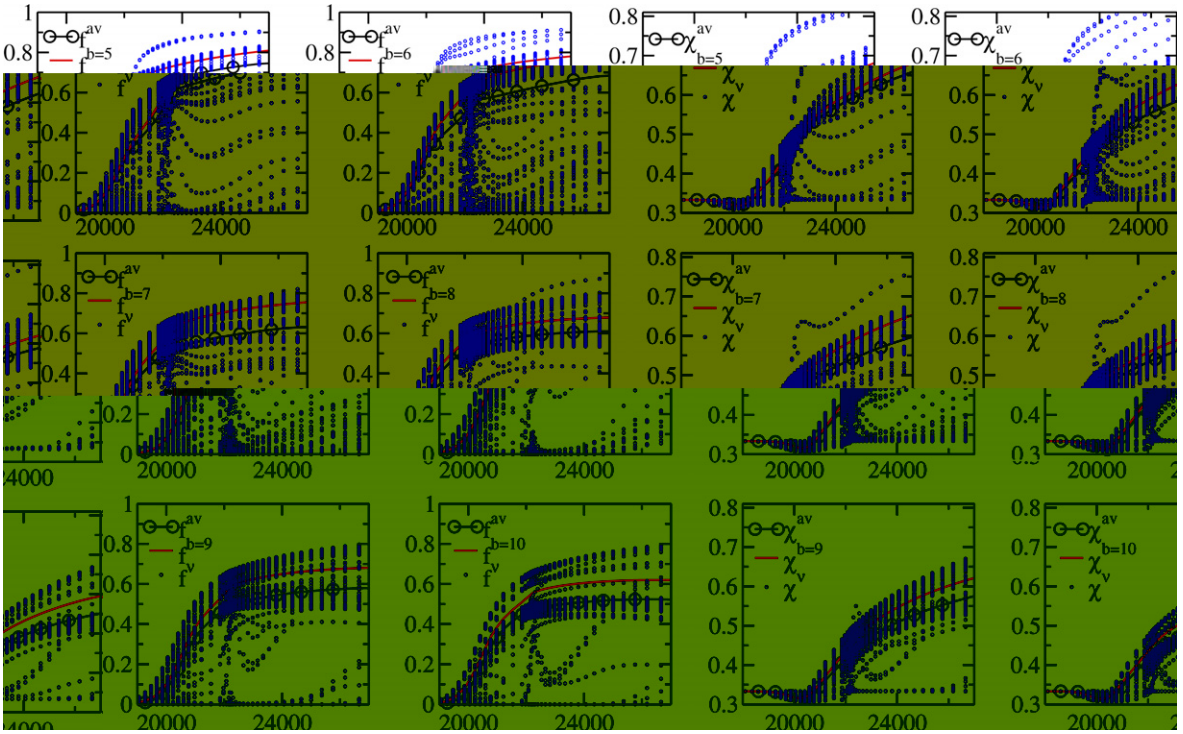

Fig. 25. AA with 21 occupied bins. Plots of the ν-values, the bin value, and the average ν-value of the anisotropy (2 columns on the left) and the Eddington factor (two columns on the right) for bin numbers 5–10.

of both Figs. 24 and 25, we plot, in each one of the sub-figures, χ^ν for all ν in the bin n (small circles), the bin value of the Eddington factor in bin i, i.e. $\chi^i = \sum_{i_k} P_R^{\nu_{i_k}} / \left(\sum_{i_k} E_R^{\nu_{i_k}} \right)$ (plain curve), and the average $\chi^{\mathrm{av}} = 1/N_i \sum_{i_k} \chi^{\nu_{i_k}}$ (curve with large circles). Again, comparing the plain curve with the curve annotated with large circles gives the accuracy of the approximation made in Eq. (36).

All comparisons must be done at a given radius to be meaningful. For instance, the 5th bin in Fig. 25 contains anisotropies mostly around 0.7–0.8 at a radius of $r = 24$ km (a nearly transparent bin), while the 10th bin contains anisotropies mostly around 0.4–0.5 (a more opaque bin) at this same radius. The reader should also not be misled by the following visual artifact: in the plots, many of the small circles represent multiple f^ν's or χ^ν's drawn on top of each other. The superposition cannot be detected by eye. However, the reader can see in Fig. 11 (right) for the solar atmosphere (and in Fig. 23 (right) for the artificial atmosphere) the actual number of frequencies in the bin and so get an idea of the number of superposed values. The mean value (curve with large circles) also gives an indication of which values of f^ν (or χ^ν) superpose. However, the average value is only computed for frequencies in $[0.2, 3] \times 10^4$ Å for the sun and in $[0.1, 6] \times 10^4$ Å for the artificial atmosphere. This is done in order to account only for those anisotropies (or Eddington factors) computed from a non-negligible intensity. In Figs. 24 and 25, in comparing the two plain curves, it can be seen that overall the approximations $f^i \simeq f^{av}$ and $\chi^i \simeq \chi^{\mathrm{av}}$ are valid. In the case of the sun and of transparent bins ($i = 5, 6, 7$), the approximation $f^i \simeq f^{\mathrm{av}}$ is rough (particularly for $i = 5$). However $\chi^i \simeq \chi^{\mathrm{av}}$ is a reasonable approximation in all cases, except for $i = 5$ where we found it crude.

The results are much better for the artificial atmosphere. Comparing the two curves, it can be seen that $f^i \simeq f^{\mathrm{av}}$ and $\chi^i \simeq \chi^{\mathrm{av}}$ are valid. Additionally, we see that the f^ν and χ^ν are less scattered from their mean values. Here, one could even assume that $f^i \simeq f^\nu$ and $\chi^i \simeq \chi^\nu$ (which would be rough for f^i for $i = 5, 6, 7$). Note that such an approximation is never used in the paper. When looking at the plots as a sequence over the bin number (for a given radius), we can see that the binning sorts the rays by decreasing anisotropies and Eddington factors as expected.

6.4. Summary of all results

- The Wien form of the pseudo-intensity has been found to be an accurate approximation of the intensity when used to derive a closure model. It also confirms that the maximum entropy closure is a valid concept.
- The mathematical approximations used to derive the by-bin closure model have been tested numerically and have been found admissible on both a 1D spherically symmetric atmosphere of the sun and an artificially complex 1D spherically symmetric atmosphere. The values of the anisotropy and Eddington factor in the bin can be approximated by their average values in the bin.
- The binning regroups the photons/neutrons according to their travel regime.
-

tially or temporally non-constant opacities is needed. The closure remains unchanged in that case, and our next effort will be oriented in this direction.

References

[1] R. Siegel, J. Howell, Thermal Radiation Heat Transfer, fourth ed., Taylor & Francis, New York/London, 2002.
[2] G.C. Pomraning, The Equations of Radiation Thermodynamics, Pergamon Press, 1992.
[3] D. Mihalas, B. Mihalas, Foundations of Radiation Hydrodynamics, Dover, 1999.
[4] M.Z. Jacobson, Fundamentals of Atmospheric Modeling, Cambridge University Press, 1997.
[5] M.F. Modest, Radiative Heat Transfer, second ed., Academic press, 2003.
[6] J.H. Ferziger, P.H. Zweifel, The Theory of Neutron Slowing Down in Nuclear Reactors, The MIT Press, Cambridge, 1966.
[7] B. Davison, Neutron Transport Theory, Oxford University Press, 1958.
[8] K.H. Beckurts, K. Wirtz, Neutron Physics, Springer Verlag, Berlin, 1964.
[9] D. Levermore, Relating Eddington factors to flux limiters, J. Quant. Spectrosc. Radiat. Transf. 31 (2) (1984) 149–160.
[10] I. Muller, T. Ruggeri, Extended Thermodynamics, Springer-Verlag New-York Inc., 1993.
[11] G.C. Pomraning, Flux limiters and Eddington factors, J. Quant. Spectrosc. Radiat. Transf. 27 (1981) 321–334.
[12] D. Levermore, G.C. Pomraning, A flux limited diffusion theory, Ap. J. 248 (5) (1982) 517–530.
[13] D.S. Kershaw, Flux Limiting Nature's Own Way: A New Method for Numerical Solution of the Transport Equation, LLNL Report UCRL-78378, 1976.
[14] T.S. Axelrod, P.F. Dubois, C.E. Rhoades, An implicit scheme for calculating time- and frequency-dependent flux limited radiation diffusion in one dimension, J. Comput. Phys. 54 (1984) 205–220.
[15] V.Ya. Gol'din, A quasi-diffusion method of solving the kinetic equation, USSR Comput. Math. Math. Phys. 4 (6) (1964).
[16] Y.B. Zel'dovich, Y.P. Raizer, Physics of Shock Waves and High-temperature Hydrodynamic Phenomena, Dover, 2002.
[17] J.-F. Ripoll, A.A. Wray, A half moment model for gray radiation and its reduction to a full moment model, J. Quant. Spectrosc. Radiat. Transf. 93 (2005) 473–519.
[18] J.-F. Ripoll, A.A. Wray, On the Pressure Closure Models, in: Proceedings of the International Symposium of Radiation Transfer, RAD-IV, Istanbul, 2004.
[19] J.-F. Ripoll et al., Modeling radiative transfer for the lightning return stroke channel, in: Proceedings of the Eurotherm 78 on Computational Radiation and Participating Media, Poitiers, Ed. Lavoisier, 2006, pp. 135–144.
[20] P.N. Brown, D.E. Shumaker, C.S. Woodward, Fully implicit solution of large-scale non-equilibrium radiation diffusion with high order time integration, J. Comput. Phys. 204 (2005) 760–783.
[21] R.B. Lowrie, A comparison of implicit time integration methods for nonlinear relaxation and diffusion, J. Comput. Phys. 196 (2004) 566–590.
[22] C. Buet, B. Despres, Asymptotic preserving and positive schemes for radiation hydrodynamics, J. Comput. Phys. 215 (2006) 717–740.
[23] R. Glowinski, J. Toivanen, A multigrid preconditioner and automatic differentiation for non-equilibrium radiation diffusion problems, J. Comput. Phys. 207 (2005) 354–374.
[24] V. Mousseau, D.A. Knoll, W.J. Rider, Physics-based preconditioning and the Newton Krylov method for non-equilibrium radiation diffusion, J. Comput. Phys. 160 (2000) 743–765.
[25] R. L Bowers, J.R. Wilson, Numerical Modeling in Applied Physics and Astrophysics, Jones & Bartlett, Boston, 1991.
[26] D.Y. Anistratov, Consistent spatial approximation of the low-order quasidiffusion equations on coarse grids, Nuclear Sci. Eng. 149 (2005) 138–161.
[27] G.N. Minerbo, Maximum entropy Eddington factors, J. Quant. Spectrosc. Radiat. Transf. 20 (1978) 541–545.
[28] T.A. Brunner, J.P. Holloway, One-dimensional Riemann solvers and the maximum entropy closure, J. Quant. Spectrosc. Radiat. Transf. 69 (2001) 543–566.
[29] M. Anile, S. Pennisi, M. Sammartino, A thermodynamical approach to Eddington factors, J. Math. Phys. 32 (2) (1991).
[30] J. Cernohorsky, L.J. Van Den Horn, J. Cooperstein, Maximum entropy Eddington factors in flux-limited neutrino diffusion, J. Quant. Spectrosc. Radiat. Transf. 42 (6) (1989) 603–613.
[31] J. Fort, Information-theoretical approach to radiative transfer, Phys. A. 243 (1997) 275–303.
[32] B. Dubroca, A. Klar, Half-moment closure for radiative transfer equations, J. Comp. Phys. 180 (2) (2002) 584–596.
[33] R. Turpault, M. Frank, B. Dubroca, A. Klar, Multigroup half space moment approximations to the radiative heat transfer equations, J. Comp. Phys. 198 (1) (2004) 1363–1371.
[34] K. Jensen, J.-F. Ripoll, A.A. Wray, D. Joseph, M. El Hafi, On various modelling methods for radiation in fires, Combus. Flame 148 (4) (2007) 263–279.
[35] R. Turpault, A consistent multigroup model for radiative transfer and its underlying mean opacities, J. Quant. Spectrosc. Radiat. Transf. 94 (3–4) (2005) 357–371.
[36] R. Turpault, Modelisation, approximation numerique et applications du transfert radiatif en desequilibre spectral couple avec l'hydrodynamique, Ph.D. Thesis, Univ. Bordeaux I, 2003 <http://tel.ccsd.cnrs.fr/index.php?hal-sid=6f2239e7981966e4a41cf99578a1dfdb&view_this_doc=tel-00004620&version=1>.
[37] S. Chandrasekhar, The radiative equilibrium of the outer layers of A star with special reference to the blanketing effect of the reversing layer, Mon. Not. R. Astr. Soc. 96 (1935) 21–41.

[38] S.E. Strom, R.L. Kurucz, A statistical procedure for computing the line-blanketed model stellar atmosphere with applications to the F5 IV star procyon, J. Quant. Spectrosc. Radiat. Transf 6 (1966) 59–147.
[39] R.L. Kurucz, Atlas: a Computer Program for Calculating Model Stellar Atmospheres, SAO Special Report 308, <http://adsabs.harvard.edu>, 1970.
[40] R.L. Kurucz, Model atmospheres for G, F, A, B, and O stars, Astrophys. J. Suppl. 40 (1) (1979) 1–340.
[41] D.F. Carbon, A comparison of the straight-mean, harmonic mean, and multiple-picket approximation for the line opacities in cool model atmospheres, Ap. J. 187 (1974) 135–145.
[42] F. Quercy, M. Quercy, V.G. Kunde, Opacity probability distribution functions for electronic systems of CN and C_2 molecules including their stellar isotropic forms, A&A 15 (1971) 256–274.
[43] D. Mihalas, L.H. Auer, J. Quant. Spectrosc. & Radiat. Transf. 71 (2001) 61–97.
[44] B. Baschek, W. Waldenfels, R. Wehrse, Opacity distribution in static and moving media, A&A 371 (2001) 1084–1096.
[45] L.H. Auer, R.B. Lowrie, Dispersion Analysis of Radiation/Thermal Fronts with Fully Resolved Spectral Opacity Variation, Los Alamos report, LA-UR-00-6094, 2000.
[46] R. Skartlien, A multigroup method for radiation with scattering in three-dimensional hydrodynamic simulations, Ap. J. 536 (2000) 465–480.
[47] H.-G. Ludwig, S. Jordan, M. Steffen, Numerical simulations of convection at the surface of a ZZ Ceti white dwarf, A&A 284 (1994) 105–117.
[48] A. Nordlund, Numerical simulations of the solar granulation. I. Basic equations and methods, A&A 102 (1) (1982) 1–10.
[49] R.F. Stein, A. Nordlund, Simulations of solar granulation. I. General properties, Ap. J. 499 (1998) 914.
[50] A. Nordlund, R.F. Stein, 3-D simulations of solar and stellar convection and magnetoconvection, Comp. Phys. Commun. 59 (1990) 119–125.
[51] A. Nordlund, R.F. Stein, in: L. Crivellari, I. Hubeny, D.G. Hummer (Eds.), Stellar Atmospheres: Beyond Classical Models, Kluwer, Dordrecht, 1991, p. 263.
[52] R.F. Stein, A. Nordlund, Realistic solar convection simulations, Solar Phys. 192 (1–2) (2000) 91–108.
[53] A. Vogler, J. Bruls, M. Schussler, Approximations for non-grey radiative transfer in numerical simulations of the solar photosphere, A&A 421 (2004) 741–754.
[54] A.A. Wray, J.-F. Ripoll, D. Prahbu, Computation of Radiation in the Apollo AS-501 Re-entry Using Opacity Distribution Functions, AIAA J. 45 (9) (2007) 2359–2363.
[55] A.A. Wray, D. Prabhu, J.-F. Ripoll, Opacity distribution functions applied to the CEV reentry, in: Proceedings of the 39th AIAA Thermophysics Conference, AIAA-2007-4542, 2007.
[56] D.E. Cullen, G.C. Pomraning, The multiband method in radiative transfer calculations, J. Quant. Spectrosc. Radiat. Transf. 24 (1980) 97–117.
[57] M.F. Modest, Narrow-band and full-spectrum k-distribution for radiative heat transfer: correlated-k vs. scaling approximation, J. Quant. Spectrosc. Radiat. Transf. 76 (1) (2003) 69–83.
[58] P. Riviere et al., Air mixture radiative property modelling in the temperature range 10,000–40,000 K, J. Quant. Spectrosc. Radiat. Transf. 56 (1) (1996) 29–45.
[59] L. Pierrot, P. Riviere, A. Soufiani, et al., A fictitious-gas-based absorption distribution function global model for radiative transfer in hot gases, J. Quant. Spectrosc. Radiat. Transf. 62 (5) (1999) 609–624.
[60] M.K. Denison, B.W. Webb, The spectral line-based weighted-sum-of-gray-gases model in nonisothermal nonhomogeneous media, J. Heat Transf. 117 (1995) 359–365.
[61] K. Huang, Statistical Mechanics, Wiley, 1963, cf. p. 196.
[62] R.W. Patch, Effective absorption coefficients for radiant energy transport in nongrey, nonscattering gases, J. Quant. Spectrosc. Radiat. Transf. 7 (1967) 611–637.
[63] J.-F. Ripoll, B. Dubroca, G. Duffa, Modelling radiative mean absorption coefficients, Comb. Theory Mod. 5 (3) (2001) 261–275.
[64] J.-F. Ripoll, A.A. Wray, The radiative transfer equation with mean absorption coefficients, in: Proceedings of the International Symposium of Radiation Transfer, RAD-IV, Istanbul, 2004.
[65] J.-F. Ripoll, B. Dubroca, E. Audit, A factored operator method for solving coupled radiation-hydrodynamics models, Trans. Theory Stat. Phys. 31 (46) (2002) 531–557.
[66] C. Baldwin et al., Iterative linear solvers in a 2D radiation hydrodynamics code: methods and performance, J. Comp. Phys. 154 (1999) 1–40.